Impact of the lower Jurassic Dunlin Group depositional elements on the Aurora CO_2 storage site, EL001, northern North Sea, Norway

Meneguolo, Renata; Sundal, Anja; Martinius, Allard W.; Veselovsky, Zbynek; Cullum, Alex; Milovanova, Elvira

DOI
10.1016/j.ijggc.2022.103723

Publication date
2022

Document Version
Final published version

Published in
International Journal of Greenhouse Gas Control

Citation (APA)
Meneguolo, R., Sundal, A., Martinius, A. W., Veselovsky, Z., Cullum, A., & Milovanova, E. (2022). Impact of the lower Jurassic Dunlin Group depositional elements on the Aurora CO_2 storage site, EL001, northern North Sea, Norway. *International Journal of Greenhouse Gas Control*, *119*, Article 103723. https://doi.org/10.1016/j.ijggc.2022.103723

International Journal of Greenhouse Gas Control 119 (2022) 103723

Contents lists available at ScienceDirect

International Journal of Greenhouse Gas Control

journal homepage: www.elsevier.com/locate/ijggc

Impact of the lower Jurassic Dunlin Group depositional elements on the Aurora CO_2 storage site, EL001, northern North Sea, Norway

Renata Meneguolo [a,*], Anja Sundal [b], Allard W. Martinius [c], Zbynek Veselovsky [d], Alex Cullum [a], Elvira Milovanova [e]

[a] Equinor ASA, Stavanger, Norway
[b] Department of Geosciences, University of Oslo, Norway
[c] Equinor ASA, Trondheim, Norway and Delft University of Technology, Delft, the Netherlands
[d] Eriksfiord AS, Stavanger, Norway
[e] TotalEnergies, Stavanger, Norway

ARTICLE INFO

Keywords:
Site selection and characterization
Geological storage potential
Lower Jurassic
Dunlin Group
Horda platform
Offshore Norway

ABSTRACT

Northern Lights is the CO_2 transport and storage component of Longship, the Norwegian full-scale CCS project. Injection is planned into an under-explored sloping saline aquifer in the northern North Sea, the Johansen and Cook formations of the Lower Jurassic Dunlin Group. To bridge the information gap, well 31/5-7 (Eos) was drilled. The comprehensive dataset acquired was fundamental to interpret the depositional environment and determine the scale and spatial distribution of heterogeneities, as input to 3-D models aimed at improving storage resource assessment and understanding the injected CO_2 plume behaviour over time. The interpreted gross depositional environments of the storage units are marginal- to shallow-marine, arranged in three successive fining-upwards intervals. The lower interval includes coastal deposits with mixed wave- and river influence, correlatable over a large distance, dominated by meso-scale heterogeneities. The middle interval records paralic deposits with a wave- and tidal- interplay generating higher vertical and lateral variability. The upper interval is interpreted as tidal-dominated, predominantly with cm-scale heterogeneities. The repeated fining-upwards trends are ideal for plume redistribution and efficient CO_2 storage, and the reconstructed lateral depositional trends associated with generally good properties indicate a high storage potential. The Eos well data enabled building the properties distribution model, highlighting the importance of well control for storage evaluation.

1. Introduction

The offshore exploitation license EL001 is the first area on the Norwegian continental shelf to be formally administered solely as a CO_2 storage site (NPD – Norwegian Oil Directorate, 2019). Companies Equinor, Shell and TotalEnergies were granted permission to develop the storage prospect as of 2019, and in early 2021 they formed the Northern Lights joint venture. "Aurora", within EL001, is the designated geological storage complex for the Norwegian full scale Carbon Capture and Storage (CCS) project "Longship" (Norwegian Government, 2020). CO_2 from different onshore sources (including Norcem cement factory in Brevik and The waste-to-energy plant shifted name recently Hafslund Oslo Celsio waste-to-energy plant) will be captured, liquified and transported by ship to an onshore hub, and finally fed via a submerged pipeline to an injection well for permanent sequestration in Aurora at ca. 2.5 km depth below the seabed. The project aims at completing Phase one by mid-2024 with a capacity of up to 1.5 million tonnes of CO_2 per year. CCS is a climate mitigation strategy with huge potential for upscaling in Norway, provided thorough assessments of safe geological storage sites (Halland et al., 2011).

The targeted CO_2 storage units are the Early Jurassic Johansen and Cook formations (as defined by Vollset and Doré (1984)). These saline aquifer sandstones south of the Troll Field in the Northern North Sea have been identified as suitable CO_2 reservoir candidates in previous studies (Halland et al., 2011) and recommended for further commercial development (Gassnova, 2012).

An exploration well (31/5-7, "Eos") was drilled in Q4 2019-Q1 2020, providing a valuable geological data set comprising cores and logs from

* Corresponding author.
E-mail address: renme@equinor.com (R. Meneguolo).

https://doi.org/10.1016/j.ijggc.2022.103723
Received 23 July 2021; Received in revised form 18 June 2022; Accepted 23 June 2022
Available online 6 July 2022

the reservoir/seal interval at > 2500 m depth, previously mapped only by seismic surveys within the EL001 (Fig. 1). The Eos well is multi-purpose, in the way that it confirmed the reservoir, was used for dynamic testing and will serve as a CO_2 injector (Meneguolo et al., 2020). This well added substantial value and confidence in the storage prospect, as subsurface information was previously only sparsely available from offset wells in the neighbouring fields. The closest, and only core available from the Johansen Formation until now was from well 31/2-3 in the Troll West area, located 30 km NE of Eos and only 18 m long. The nearest cored section of the Cook Formation was in Brage field (21 m core), 13 km W of Eos (Fig. 1).

The objective of this study has been to interpret and integrate new data into an updated, high-resolution depositional model for the Early Jurassic Johansen and Cook formations in the previously under-explored area within EL001 on the Horda Platform in the Norwegian North Sea (Fig. 1), as input to a 3D geomodel assessing the CO_2 plume behaviour. The acquired analyses and dataset from well 31/5-7 include: sedimentary core logs (lithology, facies), rock samples (Helium-porosity and permeability, petrography, mineralogy, grain size, biostratigraphy), petrophysical logs (density, porosity, lithology, depositional trends), image logs (transport directions, facies, lithology), temperature and pressure measurements, fluid samples. Interpreted sedimentological and Fullbore Formation MicroImager (FMI) data sets are presented in Appendices 3 to 5. In the following, geological interpretations of the integrated datasets are presented and correlated laterally, compared with previous studies of paleo depositional environments, and put into context of the stratigraphic development of the Dunlin Group. Sedimentary facies and near-well geological heterogeneities have been assessed with respect to reservoir property distribution and the effect on storage resource and performance. Added data from one new well highlights the importance of direct well information for injection planning and long-term storage performance predictions, valid for the Aurora storage complex and reservoir prospects elsewhere.

1.1. Geological setting

The first exploitation license (EL) for CO_2 storage on the Norwegian continental shelf, EL001, is located within the Horda Platform, a prominent structural high in the northern North Sea. Rotated fault blocks are delineated by N-S trending faults, with the "Aurora" storage site located 50–100 km offshore Western Norway (Fig. 1A). The EL covers an area of approximately 1400 km^2, with the first prospective injection well 31/5-7 (Eos) positioned to the south of the Troll West and Troll East giant hydrocarbon fields, on an eastward tilted structure bound by the Tusse Fault zone to the East and the Svartalv Fault zone to the West.

The current configuration of the Horda Platform derives from a sequence of rifting phases, followed by thermal subsidence (Færseth, 1996; Odinsen et al., 2000; Bell et al., 2014; Whipp et al., 2014; Duffy et al., 2015; Deng et al., 2017; Phillips et al., 2019), the most important

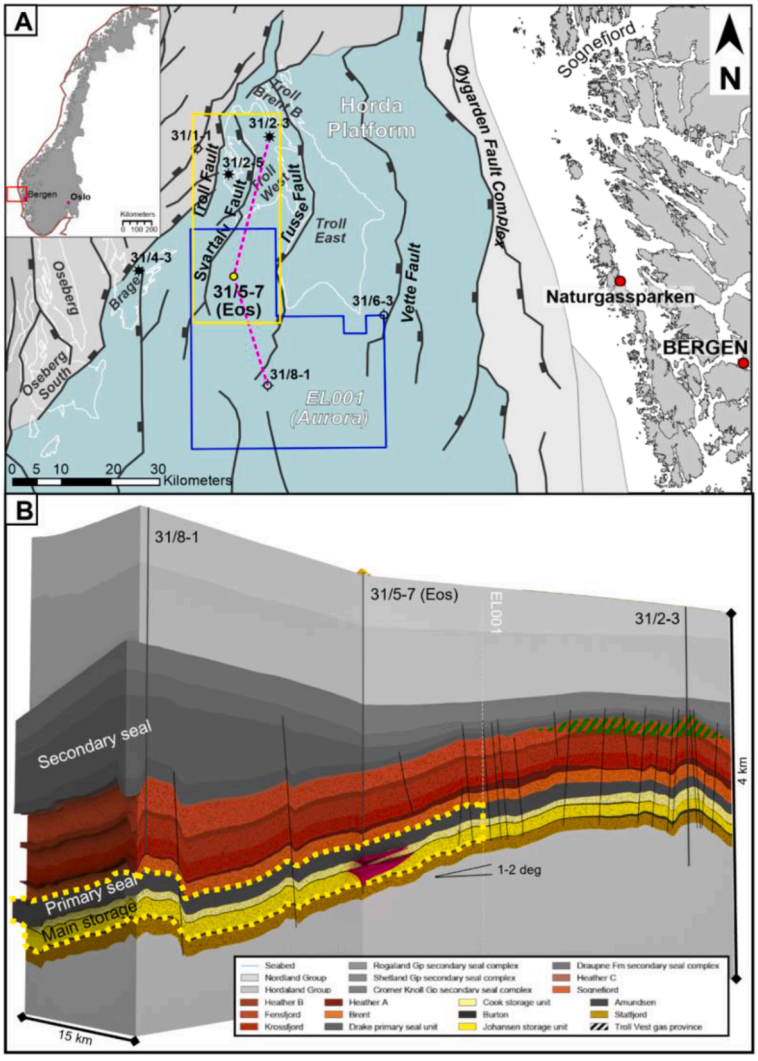

Fig. 1. A) Location map of CO_2 storage license EL001 (blue outline) in the northern North Sea, Norway. Main structural elements and faults are delineated based on data from the Norwegian Petroleum Directorate open-source fact pages (https://factmaps.npd.no). Pink dashed line: path of cross-section in Fig. 1B. Yellow rectangle: extent of the geological model grid. Circles: wells, the CO_2 injection well 31/5-7 Eos is marked in yellow. White lines: operative hydrocarbon fields. B) Section of Aurora geological CO_2 storage (vertical scale exaggeration: 10 times). Yellow dotted line: outline of lower Jurassic Dunlin Group Storage complex. Main storage: Johansen and Cook formations (marginal-to shallow-marine); primary seal: Drake Formation (marine). Pink: prediction of expected CO_2 plume extent after injection of the planned project Phase one volumes. Illustration by Equinor, based on CCG seismic data.

being a E-W extension during the Permian-Early Triassic, with the development of N-S- and NW-SE-orientation of main basin bounding and intra-basinal faults (Vette, Svartalv and Troll Fault zones, Fig. 1A). The following Middle Jurassic-Early Cretaceous phase, originating the NW-SE-striking faults, affected the Horda Platform to a lesser extent (Færseth, 1996; Bell et al., 2014; Whipp et al., 2014; Deng et al., 2017).

The stratigraphic interval of interest for the Northern Lights project is the Early Jurassic Dunlin Group (Halland *et al.*, 2011; Gassnova, 2012), deposited in a period of tectonic quiescence in the Horda Platform accompanied by a general slow sea-level rise, punctuated by short-term eustatic falls (Hallam, 2001; Figs. 1B; 2A). The Dunlin Group records deposition in a shallow-to marginal-marine setting and it includes four composite units with alternated sandstones and shales. From the base, the shales of the Amundsen Formation progressively grade into the Johansen Formation sandstones. These are followed by the heterolithic Cook Formation and capped by the Drake Formation (Vollset and Doré, 1984). For the Northern Lights project, the Johansen Formation represents the injection target and primary storage unit. The Cook Formation represents the secondary storage unit, and the Drake Formation the cap rock.

The sandstones of the Johansen Formation are present in the eastern and central Horda Platform, pinching and shaling out westwards, between the Troll and Brage/Oseberg fields (Fig. 2B).

The Johansen Formation is described as high-energy shallow-marine sandstones by Vollset and Doré (1984), and subsequently interpreted as a westward- and northwards-prograding delta (Marjanac, 1995; Marjanac and Steel, 1997) or as estuary (Charnock, 2001), based on wireline log trends, the relationship with the adjacent basinal fines deposits of the distal Amundsen Formation, and geophysical observations. More recent studies (Sundal et al., 2016) also including 3D seismic data, indicate the Sognefjord area as the main sediment source for the Johansen Formation deposits (Fig. 1A), a general westward protruding progradation (i.e. a deltaic system) with a southward, current-driven transport component.

The Cook Formation is present in a larger area than the Johansen Formation, extending across the Horda Platform to the north, west, and south (Husmo et al., 2003) (Fig. 2B). Available literature (Dreyer and Wiig, 1995; Folkestad et al., 2012; Churchill et al., 2017) focuses mostly on the Tampen Spur, a different structural element in the Norwegian North Sea ca. 100 km to the NW of the Horda Platform. The unit has been interpreted as a highly heterogeneous tidal- and wave-influenced succession (Livbjerg and Mjøs, 1989; Steel, 1993; Dreyer and Wiig,

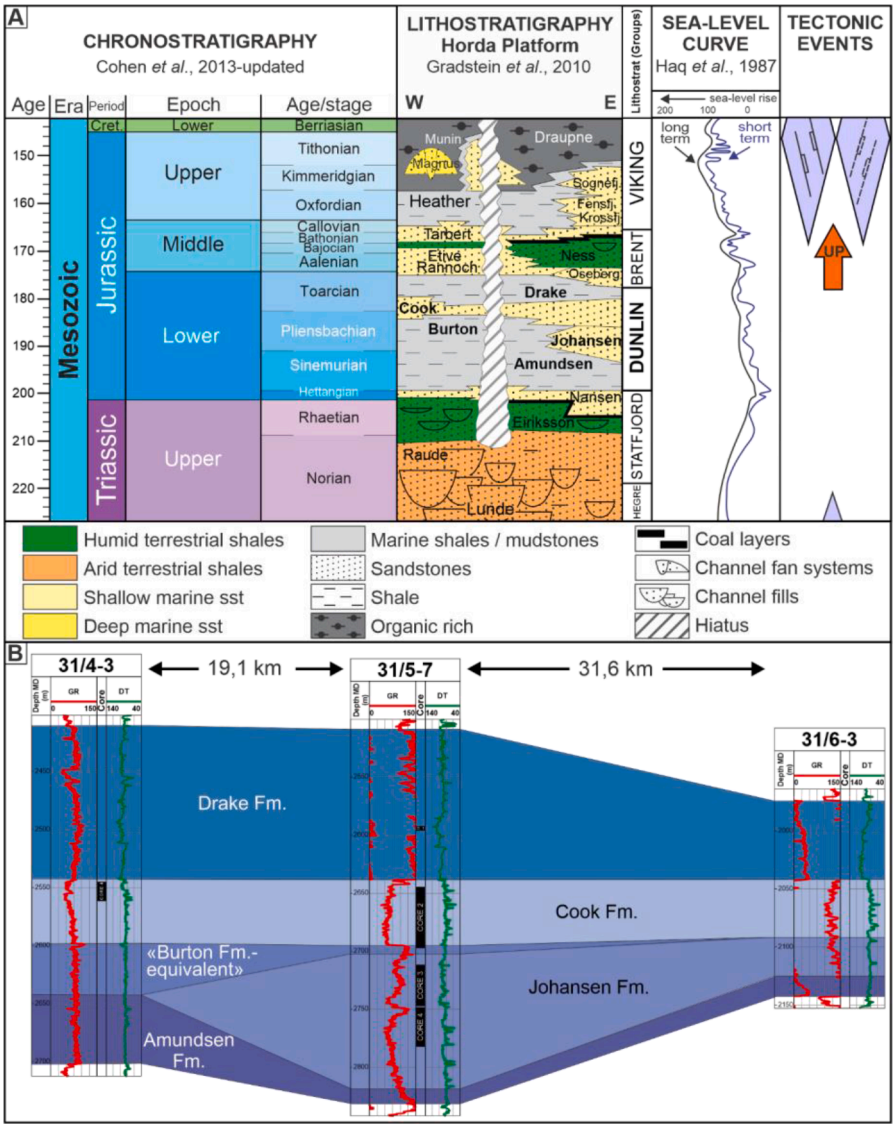

Fig. 2. (A) Chrono- and litho-stratigraphic column of Early Mesozoic in the Horda Platform. The Sinemurian to Toarcian Dunlin Group was deposited in a period of tectonic quiescence. (B) E-W (proximal-distal) correlation of the Dunlin Group across EL001. Location of wells in Fig. 1A. Chronostratigraphic chart after Cohen et al. (2013); lithostratigraphy after Gradstein et al. (2010).

1995; Marjanac and Steel, 1997) organized in a series of regional regressive – transgressive cycles (Marjanac and Steel, 1997). Churchill et al. (2017) observed tidal deposits in the lower part and wave deposits in the upper part, while Dreyer and Wiig (1995) and Folkestad et al. (2012) recognized wave-deposits in the lower part followed by tidal deposits.

The Cook Formation directly overlies the Johansen Formation sandstones only in the eastern part of the Troll West field and in the Troll East field area. In the western part of the Troll West field, a mudstone or siltstone level separates the Johansen Formation from the Cook Formation and has been interpreted as a flooding (interfingering of the Amundsen Formation) (Parkinson and Hines, 1995; Marjanac and Steel, 1997; Sundal et al., 2016). Here it is referred to as a lateral equivalent to the Burton Formation, although previously not recognized in the Horda Platform (Vollset and Doré, 1984) (Figs. 2B; 3). See 4. Discussion.

The top seal is represented by the marine mudstones of the Drake Formation, observed throughout the East Shetland Basin and the Horda Platform (Vollset and Doré, 1984), with an average thickness of 100 m in the Troll West area.

2. Database and methods

The geological investigation of the Dunlin Group storage units in the 31/5-7 well has been carried out with the integration of standard electric logs (Gamma Ray, Neutron Porosity, Density, Sonic), core observations (total 126 m of cores in the Johansen and Cook formations), biostratigraphic information (>60 samples in total from core and cuttings) and borehole image logs. A summary of the datasets in the interval of interest is displayed in Fig. 3, while the full resolution sedimentological and FMI data sets are provided in Appendices 3, 4 and 5.

Standard log suites have been utilized to infer grain size and porosity trends in intervals not covered by cores, and as correlation tool to the legacy wells. Log patterns are interpreted to reflect depositional changes.

Four cores have been cut in the Dunlin Group Storage Complex in well 31/5-7. The first one, with only 3.3 m recovery, in the Drake Formation shales. The second one, 53 m long, spans the whole Cook Formation Cores nos. 3 and 4 (35.9 and 34 m recovered, respectively) have been continuously cut in the Johansen Formation, and encompass approximately two thirds of its thickness. Cores have been utilized for visual sedimentological inspection and for direct measurements such as porosity, permeability, grain size and sorting (sieve analyses), for petrological assessment (composition, diagenesis), and for biostratigraphic analysis. Helium porosity and permeability measurements were collected with a 0.25 m interval on horizontal core plugs, and measurement-calibrated logs formed the basis of the petrophysical input

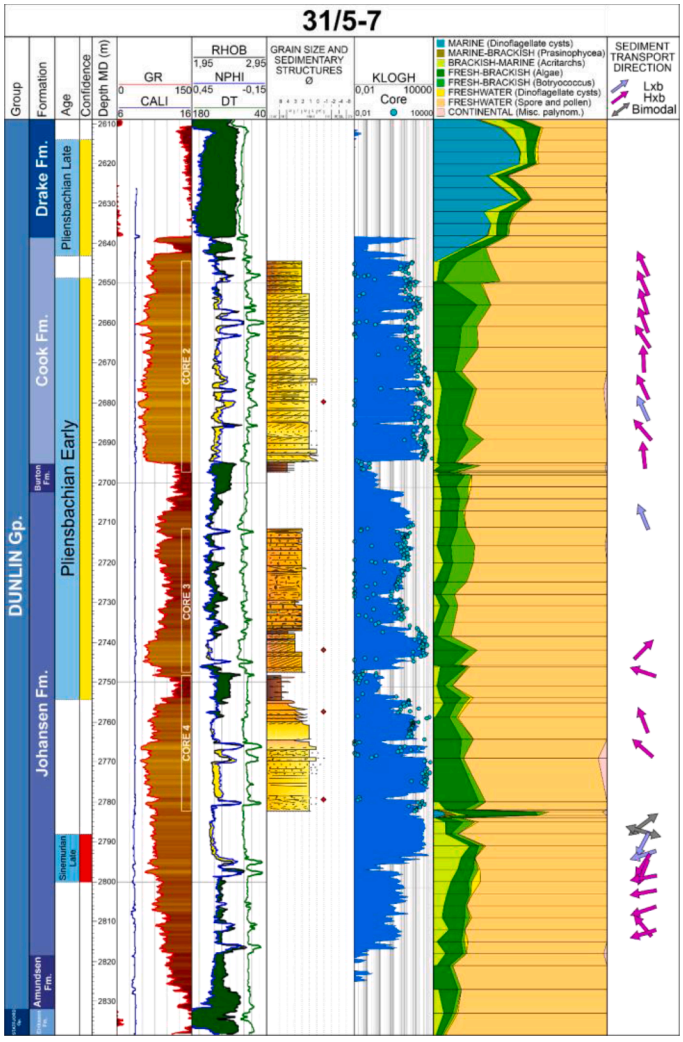

Fig. 3. Overview of the Dunlin Group in well 31/5-7 (Eos): lithostratigraphic subdivision, age, wireline log response, simplified core description, permeability log (computed and measured from core plugs), paleoenvironmental information from biostratigraphy and sediment transport direction from FMI (interval mean, see Fig. B of Appendix 1). Biostratigraphy confidence levels: red = low; yellow = medium; green = high. Red diamonds: location of thin section samples in Fig.12. Three fining-upwards sequences can be identified, with progressive rotation of sediment transport direction from W-SW to N.

to the 3D reservoir model.

Biostratigraphic data provided the chronostratigraphic framework for large-scale correlation, and information on the paleoenvironment at time of deposition based upon salinity indicators. Paleoenvironmental categories have been recognized, listed in a proximal-distal sequence: (1) Continental / Freshwater (based on terrestrial palynomorphs, miospores and freshwater dinoflagellate cysts), (2) Fresh-brackish (algae, including *Botryococcus*), (3) Brackish-marine (acritarchs and Prasinophycea) and (4) Marine (based on dinoflagellate cysts).

Fullbore Formation MicroImager (FMI) provides high-resolution resistivity images around the borehole wall which are spatially oriented in 3D. Borehole images bridge the gap between core, standard log suite and seismic information. The tool has been deployed in the 31/5-7 well with the goal of acquiring information on both (1) the structural configuration of the basin at time of deposition; (2) the depositional facies in the intervals not covered by the core, and (3) the sediment transport direction. More details are illustrated in Appendix 1. Incorporation of borehole image logs and other information for subsurface evaluation has been utilized with outcrop calibration by Hoecker et al. (1990) and by Donselaar and Smith (2005), and with core integration by Amer et al. (2011), and by Folkestad et al. (2012) for the Cook Formation in the Tampen Spur area.

The acquired 31/5-7 datasets have been utilized to distinguish lithofacies, facies associations and depositional elements, and to reconstruct the depositional history of the Dunlin Group, with the aim of delineating large-, meso-and small-scale geological heterogeneities, as well as reservoir properties distribution within the storage complex. This information constituted the input to a static and dynamic 3D geomodel, built in the RMS^{TM} and Eclipse 300^{TM} software respectively, used to quantify storage resources in the Aurora storage complex considering plume development in time and space for the planned injection of 1,5 Mtpa over 25 years and after injection stop.

The experimental design encompassed a stochastic ensemble of 400 realizations within an uncertainty span, and main geological factors impacting flow have also been analysed as single sensitivities. A lateral grid cell size resolution (200 m x 200 m) was chosen as a reasonable balance between the simulation time and the level of the details on the CO_2 plume distribution. The average vertical grid cell size is 4 m. The vertical grid resolution was increased for the layers located beneath a potential baffle or barrier to capture the impact of potential high permeability streaks. As thickness of the relevant units was below seismic resolution, the grid was constructed as proportional, based on well picks. The geomodel spans an area of 710 km^2 (Fig. 1) and includes ca. one million cells. Regionally connected Dunlin Group pore volume outside the gridded area has been implemented in the dynamic model using numerical aquifer option. The CO2STORE option, specifically designed in Eclipse 300 for modelling of CO_2 storage in saline aquifers, was used for the dynamic simulations. Three phases were considered: a CO_2-rich phase, an H_2O-rich phase, and a solid phase (salts). Mutual solubilities of CO_2 and H_2O are calculated to match experimental data for a CO_2 - H_2O system under typical CO_2 storage conditions based on the models by Spycher and Pruess (2005, 2009) (Schlumberger, 2021). Dissolution rate of CO_2 was therefore not directly inputted to the simulations, although brine salinity affects the amount of CO_2 dissolved in water. Salinity from fluid samples in well 31/5-7 (4,3 mol%) was used as input. Reservoir conditions derived from the Eos well database are 107°C and 271 bara (hydrostatic) at 2670 m TVDSS. Irreducible water saturation was derived from Viking Group analogues.

Based on this data, four (4) different relative permeability models have been made representing low, moderate, high and very high mobilities for CO_2 to cover the uncertainty span for CO_2 mobility in the storage formations. Both shape parameters (LET) and endpoints for these models were taken from CO_2 analogues. One relative permeability model is applied to the whole reservoir model. All simulations were run with hysteresis as default, i.e., with both drainage and imbibition curves for CO_2 (no imbibition curves for water) in order to account for residual gas trapping.

Integration and interpretation of new data in this way is crucial for assessing the injectivity and fluid pathways for CO_2, as well as the immobilization potential, storage security and resource.

3. Results

3.1. Lithofacies and facies associations

Seventeen lithofacies were defined based on sedimentological and ichnological core observations, integrated with grain size and sorting from core measurements and petrophysical logs. Lithofacies are summarized in Table 1 and assigned identifiers based on appearance characteristics. Eight facies associations (FA) were interpreted, representing changing environments in a shallow- to marginal-marine succession. Due to the significant distance between offset wells and lack of core information, several alternative interpretations are provided in some instances.

The FA are representative of three depositional environments: coastal, paralic and shallow-marine. From the bottom (oldest part of the succession) and upwards, the identified facies associations are:

Coastal FA: sediments deposited in a marginal marine setting, subject to wave/current and gravity depositional processes. The subaqueous distributary channel FA and mouth bar FA belong to this group.

Paralic FA: deposits found on the landward side of a coast or in shallow marine water, susceptible to marine invasions, resulting in interfingered marine-and non-marine deposits. The FA belonging to this group are lower and upper intertidal flat FA, tidal inlet/flood tidal delta FA, upper subtidal flat FA and tidal channel FA.

Shallow-marine FA: sediments deposited in a marine setting, on a shelf with variable water depth. The compound dune FA is representative of this environment.

3.1.1. Subaqueous distributary channel FA

This FA is present at the base of core no. 4 and is mostly constituted by m-thick lithofacies Xco with intercalation of lithofacies CC, and by dm-thick stacks of lithofacies Xmh and Xml. Additionally, this FA is composed of massive to plane-parallel laminated sandstones (lithofacies Sm), well-sorted (average sorting index 0.59), with a fining-upward trend to lithofacies Xf and Xfo (Fig. 4A).

The Xco lithofacies (Appendix 5) display normal grading, small-scale cross-stratification and secondarily wave- and bidirectional ripples. This lithofacies fines upwards to a dm-thick interval of lithofacies CC, highly bioturbated, with marine bioclasts (belemnites, bivalve fragments). Sediment transport direction from FMI display a W-ly and S-ly component, with a bimodal interval (Fig. 3, Appendix 5). The high- and low-angle cross-stratified sandstones lithofacies record sustained unidirectional flow towards the W and WNW. The stack displays a trend of decreasing foreset inclination and of set thickness uphole from FMI (Appendix 5). This is interpreted as decreasing energy and water depth, compatible with the gradual infilling of a channel.

The massive to faintly laminated sandstones (Sm) display occasional bioturbation and traction lamination, not fully resolved in the FMI log, due to the lack of lithological contrast. This is interpreted as the product of a bank collapse feature (mass-flow process related to turbidites, *cf.* Van den Berg *et al.*, 2017).

The upwards transition towards cross-stratified sandstones (lithofacies Xf and Xfo) indicates reduced energy and higher grain size contrast (average sorting 0.76 and 0.99, respectively). These lithofacies display a NW-ly sediment transport direction from FMI (Fig. 4A). Continental influence can be inferred from the presence of organic material. Mixing of salinity is suggested by the fresh to brackish water biostratigraphic indicators and by the marine macrofossils.

The overall fining-upwards trend, coupled with the predominance of unidirectional flow with dominant W-ly transport direction and low bioturbation index suggest deposition in a channelized body, possibly in

Table 1
Lithofacies summary. Sorting is calculated as standard deviation of grain size (in Phi) from 121 core plug measurements. Abbreviations: VW, very well sorted; W, well sorted; M, moderately sorted; P, poorly sorted; VP, very poorly sorted. B.I.: bioturbation index, ranging from 0 (bioturbation absent) to 5 (fully bioturbated). Details on image facies are presented in Table B of Appendix 1. It should be noted that lithofacies CC does not fully represent a depositional facies *per se*, but rather a diagenetic imprint of bounding lithofacies.

Code	Lithology and grain size	Sorting	Sedimentary structures	Bioclasts	Trace fossils	B. I.	Lithofacies thickness	Processes	Facies association occurrence	Predominant image facies
Xc	Medium- to coarse-grained sandstones	VW (avg. 0.2) (0.17-0.24; n = 4)	Tabular low-angle to horizontal cross-stratification. Structureless in places	Rare bivalve fragments and belemnites	*Palaeophycus*	0-1	Set thickness: min 20, max 110 cm	Unimodal flow lamination	Primary: mouth bar	Slxb, Shxb, S
Xco	Medium- to coarse-grained sandstones	VW (avg. 0.33) (0.16-0.65; n = 10)	Mostly high-angle through cross-stratified sets, normal grading, organic material along lamina	Rare bivalve fragments and belemnites	*Thalassinoides, Palaeophycus, Skolithos*	0-1	Set thickness: min 10, max 50 cm	Unimodal flow lamination	Primary: subaqueous distributary channel	Slxb, Shxb
Sm	Fine- to medium-grained sandstones	M to W (avg. 0.59) (0.43-0.76; n = 9)	Structureless to faintly plane-parallel lamination	-	-	0	Min 20, max 160 cm	Upper flow regime or mass-flow	Primary: subaqueous distributary channel; Secondary: compound dunes	Sb, S
CC	Very fine- to medium-grained sandstones, calcite cemented	VW (avg. 0.35) (0.06-0.64; n = 2)	Faintly plane-parallel laminated to highly bioturbated	Abundant bivalve fragments, belemnites	*Skolithos, Ophiomorpha*	4-5	Min 7, max 85 cm	Winnowing/ abandonment	Primary: mouth bar; subaqueus distributary channel; Secondary: compound dunes, upper subtidal flat	Cem, S, Sb
M	Mudstones	N/A	Structureless to plane-parallel lamination	-	*Phycosiphon*	0-1	Min 2, max 20 cm	Deposition from suspension	Primary: lower intertidal flat	M, Ml
Hhb	Mixed very fine- to fine-grained sandstones and mudstones	P (Avg. 1.45) (1.25-1.69; n = 4)	Wave and current ripples, rare synaeresis cracks, high B.I.	-	*Taechnichnus, Planolites, Paleophycus,* bivalve traces	> 3	Min 3, max 10 cm	Sandy to mixed flat	Primary: tidal channel, lower intertidal flat. Secondary: upper intertidal flat	Hmud, Hsand
Hlb	Mixed very fine- to fine-grained sandstones and mudstones	Sandstones: P to VP (avg. 1.71) (1.33-2.10; n = 3)	Wave and current ripples, rare synaeresis cracks, lower B.I.	-	*Taechnichnus, Paleophycus,* bivalve traces	1-2	Min 4, max 20 cm	Sandy to mixed flat	Primary: tidal channel, lower intertidal flat; Secondary: upper subtidal flat	Hmud, Hsand
SMa	Alternated very fine- to fine-grained sandstones and mudstones	Sandstones: P (1.25; n = 1)	Wave and current ripples, rare synaeresis cracks	-	Undifferentiated	0-1	Min 4, max 20 cm	Mixed to mud flat	Primary: lower intertidal flat; Secondary: tidal channel	Hmud, Hsand
Sl	Fine-grained sandstones	P (avg. 1.15) (0.63-1.45; n = 5)	Unidirectional low-angle parallel laminated sets	Rare belemnites	-	0	Min 2, max 40 cm	Unimodal flow lamination, fluvial- and tidal-dominated	Primary: upper subtidal flat; Secondary: lower intertidal flat	S, Sb, Silt
SBl	Muddy sandstones, very-fine to fine-grained	P (avg. 1.12) (1.02-1.35; n = 12)	Wave and current ripples, low bioturbation index	-	*Arenicolites, Siphonichnus, Rosselia, Thalassinoides, Paleophychos.* Larger individual traces	1-2	Min 2, max 100 cm	Sandy flat	Primary: upper subtidal flat; Secondary: lower intertidal flat	Silt, Hmud
SBs	Muddy sandstones, very-fine to fine-grained	P (avg. 1.21) (0.65-1.85; n = 7)	Wave and current ripples, moderately bioturbated	-	*Arenicolites, Paleophychos*. Smaller individual traces	2-3	Min 2, max 50 cm	Sandy flat	Primary: upper subtidal flat, deep	Silt, Ssirr, Hmud

(*continued on next page*)

Table 1 (*continued*)

Code	Lithology and grain size	Sorting	Sedimentary structures	Bioclasts	Trace fossils	B. I.	Lithofacies thickness	Processes	Facies association occurrence	Predominant image facies
									intertidal flat; Secondary: lower intertidal flat, tidal channel	
Hps	Mainly mudstones and siltstones, secondarily very fine- to fine-grained sandstones	Sandstones: VP to P (avg. 1.45) (1.19-1.59; n = 3)	Pin-striped lamination, synaeresis cracks in places	-	Dominant *Taenidium* and *Teichnichnus*	1-2	Min 35, max 55 cm	Mixed to mud flat	Primary: upper intertidal flat; Secondary: lower intertidal flat	Hmud, M, Ml
Xf	Medium- to fine-grained sandstones	M (avg. 0.76) (0.56-1.17; n = 10)	Low- to high-angle through cross-stratified sets	-	Undifferentiated	0-1	Min 5, max 40 cm	Unimodal flow lamination	Primary: inlet/flood tidal delta; Secondary: subaqueous distributary channel	Slxb, Shxb, S
Xfo	Medium- to fine-grained sandstones	M (avg. 0.99) (0.93-1.06; n = 2)	Low- to high-angle through cross-stratified sets, rich in organic material	-	Undifferentiated	0-1	Min 5, max 40 cm	Unimodal flow lamination	Primary: inlet/flood tidal delta; Secondary: subaqueous distributary channel	Slxb, Shxb, S, Hsand
Xml	Medium-grained sandstones	M to W (avg. 0.55) (0.26-0.71; n = 20)	Low-angle cross-stratified tabular sets. Accretion surfaces identified in places. Muddy, finely laminated silt layers (fluid muds), on average 1 cm thick, occur with 2 m spacing decreasing upwards to ca. 0.5 m	Abundant bivalve fragments, belemnites, ammonites	*Paleophycus*	0-1	Set thickness: min 10, max 130 cm	Dune toesets. Progradation indicated by accretion surfaces.	Primary: compound dunes; Secondary: subaquoeus distributary channel	Hsand, Sb, S
Xmh	Medium-grained sandstones	M to W (avg. 0.59) (0.16-0.97; n = 29)	Low-angle cross-stratified tabular sets, normal grading, pebbly lags occur	-	-	0	Set thickness: min 10, max 180 cm	Dune foresets	Primary: compound dunes; Secondary: subaquoeus distributary channel	Slxb, Shxb, S
Sh	Bioclasts accumulation	VP	Equilibrium position, iso-orientation of elongated fragments	Predominant bivalve fragments, secondarily belemnites	-	0	Min 5, max 30 cm	Shell hash	Primary: compound dunes	-

a distributary channel. Secondary wave-ripples and tide-energy indicators are also identified. This FA is also recognized in well 31/2-3 (Troll West), in the same stratigraphic level (lower Johansen Formation) (Sundal et al., 2016) (Figs. 1 and 8).

3.1.2. Mouth bar FA

This FA is recorded in the lower part of core no. 4 and comprises lithofacies Xc and CC in m-thick coarsening upwards sequences, with sediment transport direction from FMI towards the NNW (Fig. 4A). Biostratigraphic data indicate mixing of marine- and fresh-water (marine dinoflagellate cysts and algae, Fig. 3), while marine macrofossils (belemnites) were observed in core. The well-sorted (average sorting 0.2), medium to coarse-grained lithology with low-angle cross-stratification (potentially swaley) and low levels of bioturbation indicates high-energy unimodal flow with continental influence (organic material). The highly bioturbated and cemented intervals may be interpreted as winnowing in a subaqueous setting, with marine influence. Reworking by waves in a marine setting may account for both the high degree of sorting and for the predominance of horizontal and low-angle cross-stratification. Only one high-angle cross-stratified layer is detected from FMI in the interval displayed in Fig. 4B.

Log response below the cored interval indicate an overall coarsening-upwards trend, with W-ly sediment transport direction and one bimodal interval (Fig. 3). The overall coarsening-upward trend, the stratigraphic position repeatedly within subaqueous distributary channel FA, the mixing of fresh-and marine-water indicators and of fluvial- and wave-related processes may indicate deposition in or close to a river mouth. The relative influence of fluvial and wave processes cannot be determined with confidence based on the 31/5-7 cores only. It is therefore postulated that the sedimentary environment encompassing the subaqueous distributary channel and mouth bar FA ranges between a wave-dominated delta and an upper shoreface with distributaries

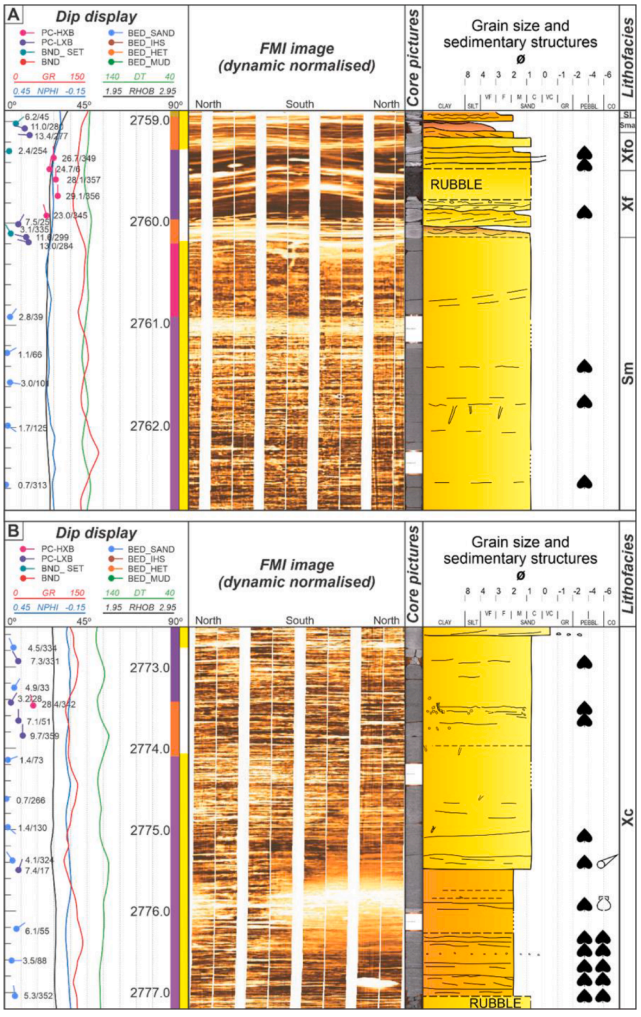

Fig. 4. Dip directions, well logs, image and core logs from well 31/5-7 in the coastal facies associations, Johansen Formation. Core symbols and FMI facies (left column) as in Appendix 2. Right column, FMI data quality: yellow, moderate image quality; white, high image quality. (A) Subaqueous distributary channel FA, dominated by massive to plane-parallel laminated sandstones (lithofacies Sm) capped by lithofacies Xf and Xfo with a fining-upward trend. Good match exists between observed faint core features and boundaries identified from FMI. (B) Mouth bar FA, dominated by medium- and coarse-grained planar to low-angle cross-stratified sandstones (lithofacies Xc).

(Dominguez, 1996; Bhattacharya and Giosan, 2003).

The mouth bar FA is also recognized in well 31/2-3 (Troll West) in the lower Johansen Formation, but above the subaqueous distributary channel FA (Sundal et al., 2016) (Figs. 1 and 8).

3.1.3. Lower intertidal flat FA

The lower intertidal flat FA occurs at the top of the lower Johansen Formation (upper part of core no. 4, 2748-2755 m), where it transitions from the subaqueous distributary channel FA and is intercalated to the inlet/flood tidal delta FA. This facies association displays an alternation of fine-grained lithofacies (lithofacies M, SMa, Hps, Hlb, Hhb) and low-energy sandy lithofacies (Sbl and Sbs; secondarily Sl). Fine-grained lithofacies display a rhythmic pattern from mixed lithologies, with a decreasing degree of bioturbation (from highly bioturbated, Hhb, to less bioturbated, Hlb) to alternated lithologies (SMa, Hps) and mudstones (M). This succession is interpreted as indicative of increasing stress conditions, potentially due to salinity oscillations, sedimentation rate variations or emersion cycles (Gingras et al., 2012; Dashtgard, 2011; Hertweck et al., 2005).

Normal-graded beds are observed in the upper part, possibly indicating deposition by individual fine-grained hyperpycnal flows.

Bi-directional ripples, single- and double-mud drapes and micro-HCS indicate both tidal and wave energy. Mixing of fresh and saline water is recorded by synaeresis cracks and by biostratigraphic data (Fig. 3). This FA is interpreted to record slightly deeper conditions than the upper intertidal FA because of the thicker sandstone interval with traction features. The increase of frequency and thickness of mudstone intervals towards the top may indicate a shallowing-upwards trend.

Due to of lack of core data in the legacy wells, the exact geomorphological location for this FA in a coastline setting cannot be precisely established. Since fluvial processes recorded in the underlying interval, an interdistributary bay sedimentary environment is postulated. Alternatively, this FA could fit an open-coast tidal flat setting, assuming that riverine input is secondary. Nevertheless, both options suggest an elongated coastline with low-energy deposits, variably intersected by riverine input, and a further accurate distinction is deemed unnecessary at this point.

3.1.4. Inlet/flood tidal delta FA

This facies association comprises lithofacies Xfo (medium to fine cross-bedded sandstones, with, high organic material content) and Xf (medium to fine cross-bedded sandstones), in a slightly coarsening-upwards trend. They erosionally (possibly unconformably) overly the lower intertidal flat deposits at the top of core no. 4, and transition upwards to the upper subtidal FA in the lower part of core no. 3. The finer grain size, the location within lower energy heterolithic intervals and the main sediment transport direction towards the NE (Fig. 3, Appendix 4) (i.e. towards the assumed direction of the main sediment source area) indicate that these features could represent a tidal inlet and potentially a flood tidal delta, similar to observations presented in Sundal et al. (2016). Occurrence of belemnites supports the connection to the open sea, while proximity to a river is indicated by few specimens of fresh-water dinoflagellates (Fig. 3). This interpreted depositional element implies the presence of a restriction, such as a barrier island or a spit, and a mixing of wave- and tide- energy (Darlymple and Choi, 2007).

Alternatively, this interval may represent thin shoreface deposits (landwards-migrating dunes in an upper shoreface) such as the ones identified by Ravnås and Steel (1998) in the Middle Jurassic in the North Sea, or in outcrop by Walker and Wiseman (1995). However, the abundance of organic matter debris and the gradual upwards transition towards the upper subtidal FA do not support this interpretation.

3.1.5. Upper subtidal flat FA

This FA is observed in the upper part of the Johansen Formation (core no. 3, Fig. 3 and Appendix 4), where it transitions from the lower intertidal FA. It comprises mostly lithofacies Sbl, Sbs and Sl, with only secondarily lithofacies Hhb and Hlb. Commonly, the lithofacies sequence Sl-SBl-SBs is observed. Wave-and current ripples are the most common features, with no reliable FMI pattern. Only towards the top of the core, low-angle cross-bedded layers display sufficient thickness for the FMI signal to allow a reliable sediment transport direction interpretation, which indicates a northernly main component (Figs. 3 and 5). Two intervals (2734.20-2727.80 m and 2726.30-2721.25 m) display a thickening-thinning upwards trend of the strata, interpreted as tidal bundles.

This FA is repeatedly intercalated by the tidal channel FA The upwards trend is recorded by logs only, as a ca. 13 m core gap is present between the top of core 3 and the base of core 2. The fining-upwards GR log trend combined with the interpreted upper intertidal FA at the base of core 2 indicates a progradational pattern. The inferred FA succession would therefore continue with lower intertidal deposits (inferred from log in the gap between cores nos. 3 and 2).

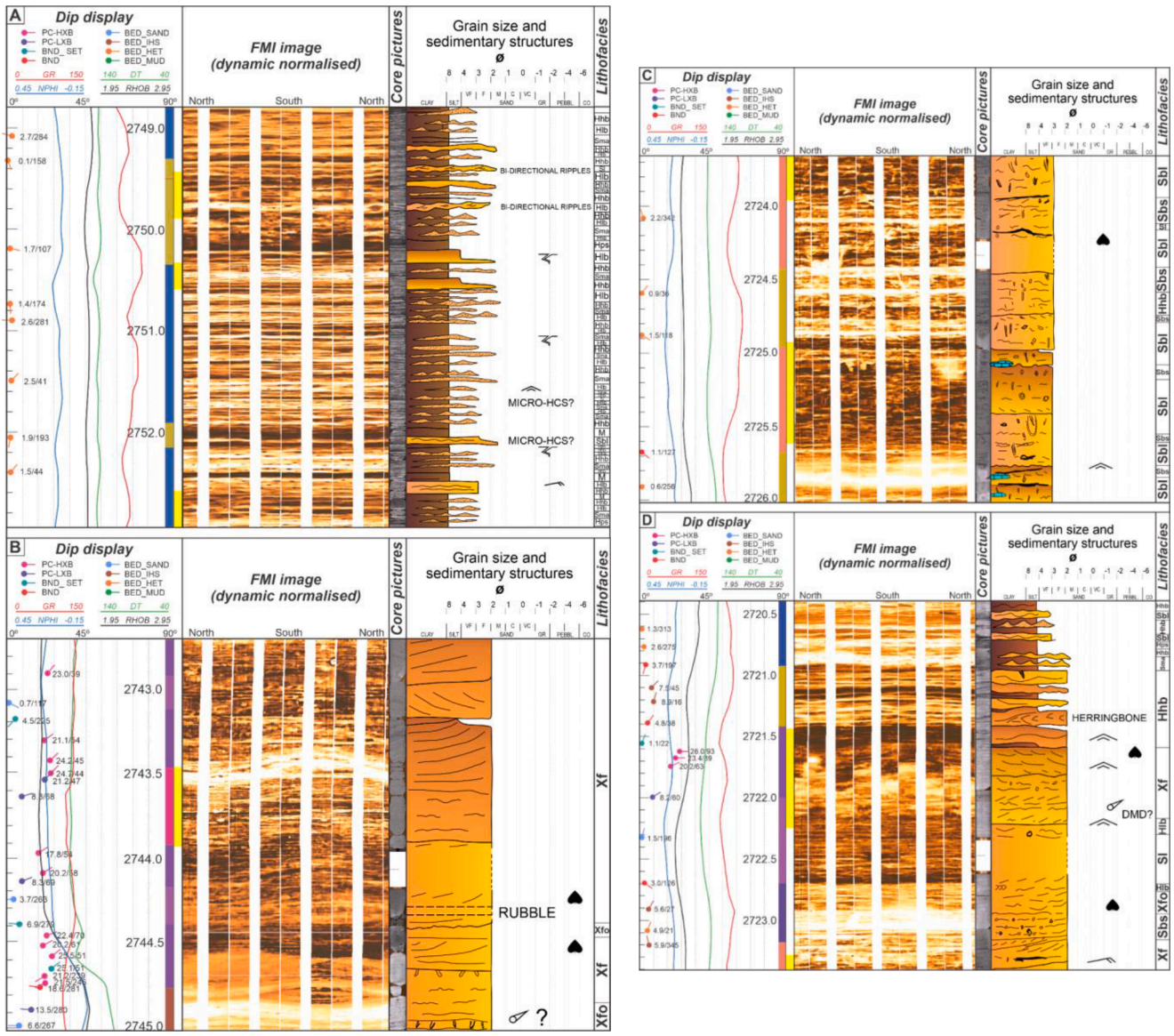

Fig. 5. Dip directions, well logs, image and core logs from well 31/5-7 in the paralic facies associations, Johansen Formation. See previous figure for explanation. (A) Lower intertidal flat FA. Due to scale of sedimentary features, core provides higher detail than FMI; (B) Tidal inlet/flood tidal delta FA. A minor stick-and pull event (uneven measurement of the FMI wireline tool) occurs in the uppermost part (between 2743.2 and 2742.9 m ca.). HCS = Hummocky cross stratification.

3.1.6. Tidal channel FA

This FA is observed in the upper part of the Johansen Formation, interbedded with the upper subtidal flat FA. The tidal channel FA is predominantly composed of Xf, Xfo and Sbs lithofacies, overlain in places by Hhb, Hlb, Sbs, and SMa lithofacies. Dm-to m-thick stacks of lithofacies Xf, Xfo and Sbs with sharp base indicate sustained flow, and is be interpreted as active channel fill albeit with low energy (lack of erosional base and of channel lag). Unimodal sediment transport direction towards the E and NW could be detected from FMI in the interval 2720.25-2719.70 m (Appendix 4). Lithofacies Hhb, Hlb, Sbs, SMa in dm- to cm thick intervals directly overlying the cross-laminated sandstones are indicative of decreasing energy and could be interpreted as the passive channel fill.

Frequency of active tidal channel FA occurrence within the upper subtidal flat FA increases upwards and is accompanied with a thickness decrease, possibly indicating a shallowing-upwards trend, in accordance with the progradational pattern inferred by the log and core response of the upper part of core no. 3 to the base of core no. 2 (upper subtidal flat FA).

3.1.7. Upper intertidal flat FA

This facies association is predominantly constituted by lithofacies Hps, which represent the finest grain size fractions and lowest energy lithologies (deposition from suspension of siltstone and shales mm- to cm- thick intercalations of lenses with rippled fine sandstones). Secondarily, lithofacies Hhb is identified (Fig. 6A). This FA is observed at the base of core no. 2, at the transition between the Johansen and the Cook formations, at the culmination of a fining-upward trend from the upper subtidal flat FA at the top of core no. 3 (Fig. 3).

The reduced ichnological diversity, the lack of rootlets and the fresh- to brackish-water influence identified based on biostratigraphic data (Acritarcs and Dinoflagellate cists, Fig. 3) support the interpretation of a shallow intertidal depositional environment, protected from riverine input.

Fig. 5 Dip directions, well logs, image and core logs from well 31/5-7 in the paralic facies associations, Johansen Formation, continued. See previous figure for explanation. (C) Upper subtidal flat FA. Only small-scale sedimentary features interpreted from FMI, but individual trace fossils can be identified. Repeated thickness variations (upward

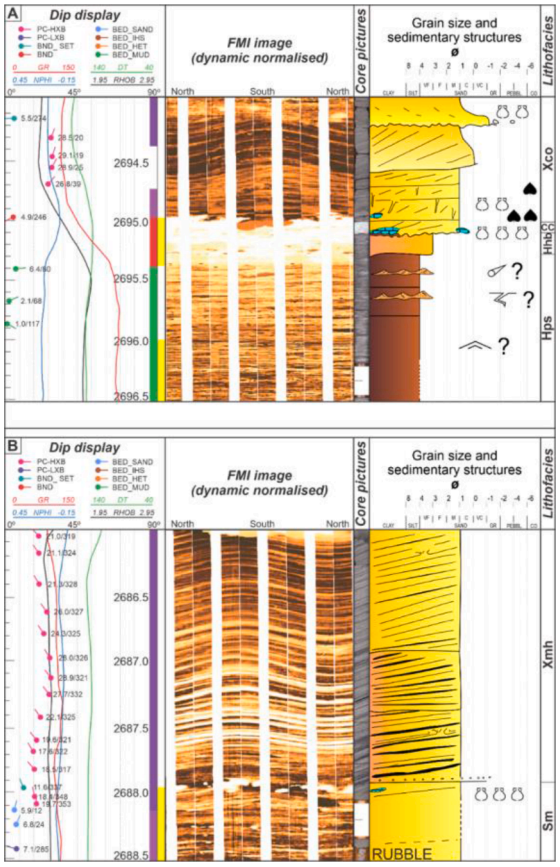

Fig. 6. Dip directions, well logs, image and core logs from well 31/5-7 in the shallow-marine facies association, Cook Formation. See Fig. 4 for explanation. (A) Boundary between compound dune FA (base of Cook Formation) and upper intertidal flat FA (dominated by lithofacies Hps), lateral equivalent of the Burton Formation. Complete congruence exists between FMI and core facies: cross-stratification in the Cook Formation and pin-striped to lenticular bedding in the "Burton Formation-equivalent". (B) Compound dune FA, with multiple sets of high-angle cross-stratified sandstones (lithofacies Xmh), and secondarily structureless sandstones (lithofacies Sm). Increasing then decreasing cross-stratification angle can be observed in the FMI log. However, in the displayed interval set boundaries are far easier to distinguish in the core.

decreasing cycles) at dm-scale may represent tidal bundles. (D) Tidal channel FA. Fining-upwards sequence from flow-laminated facies (channel base) to bioturbated heterolithics (channel abandonment). A stick-and pull event (uneven measurement of the FMI wireline tool) can be detected in the middle part (between 2721.75 and 2722.10 m ca.) DMD = Double mud drapes.

3.1.8. *Compound dunes FA*

The Cook Formation in well 31/5-7 (core no. 2) is composed uniquely of this facies association. The onset of the unit is possibly unconformable above the pin-striped heterolithics (upper intertidal flat FA) of the "Burton Formation-equivalent" (Fig. 6A) and is marked by a calcium carbonate-cemented interval (lithofacies CC. See comment in Table 1). Although no age gap is recorded across this surface (Fig. 3), the erosive nature and the cementation may be indicative of an unconformity.

The base of the Cook Formation is represented by a 4.5 m-thick alternation of cross-bedded sandstones with organic material and shell debris (lithofacies Xco), and high-angle and low-angle cross-stratified sandstones (lithofacies Xmh and Xml). The main expression of the compound dunes FA is the stack of dm- to m-thick tabular cosets formed by toeset (Xml)-foreset (Xmh) transition and parallel set contacts, interbedded in place with secondarily dm-to m-thick structureless sandstones (lithofacies Sm) (Fig. 6B) and cm-thick shell hash deposits (lithofacies Sh). Fluid muds (mm- to cm-thick) also occur. Dm- to m-thick cemented layers (lithofacies CC) are identified in several occurrences (Fig. 3 and Appendix 3), with increasing frequency and thickness in the upper part of the unit (above 2667 m core depth). They are often associated to bioclasts accumulation and could indicate a temporary halt in sedimentation or abandonment, allowing for growth and development of mollusc banks. Lithofacies CC represents a secondary diagenetic imprint, where the carbonate source is dissolved and reprecipitated in sands deposited below or above, typically cementing lithofacies Sm or Xml. In the uppermost part of the Cook Fm., accretion surfaces can be observed, and fluid muds are recorded more frequently, indicating mixing of fresh- and saltwater and an associated increase in tidal influence. Grain size decreases from fine to medium down to very fine to fine. Toeset/foreset pairs become thinner, indicative of waning energy and/or shallowing water depths (Fig. 7). The thickness of the toesets/foresets couples displays two cycles of upwards decrease, followed by an upwards increase. (Fig. 7). The succession is therefore interpreted as a series of compound dunes bedforms in a high energy environment.

The sediment transport direction of this FA displays a low degree of variability in the lowermost part of the succession, with mainly N- and NNW-ly direction with subordinate NNE-ly component from high-angle cross-stratification (Fig. 6A), then becoming unimodal towards the N-NW. A consistent angularity of 5-20° is detected between the NNW palaeocurrents from cross-sets and the measured bedform symmetry from the plane-parallel bedded units (approximatively N-S), resulting in an overall dune accretion direction sub-parallel to the prevailing flow (Figs. 3; 6B).

The high-energy deposits in a deeper water setting coupled with the recorded sediment transport direction may indicate deposition in a submerged dune field or ridge in a tide-dominated setting (Olariu et al., 2012; Darlymple, 2010; Stride et al., 1982). This interpretation is

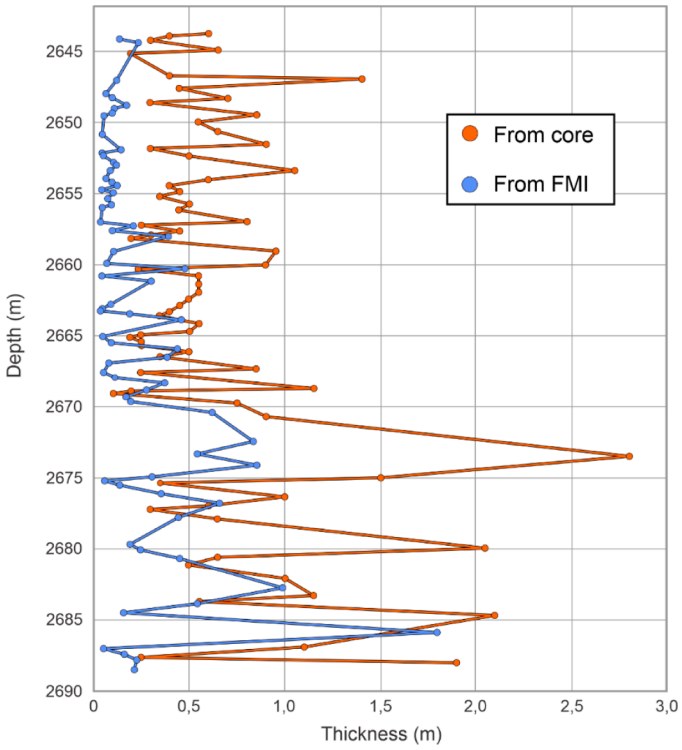

Fig. 7. Plotted toeset/foreset pair thickness for the compound dune FA in the Cook Formation from FMI and core observation (core no. 2), interval 2643-2688 m (core depth). From the base, three intervals of set thickness variations can be recognized. Observations from FMI are of higher confidence because of the 3D nature of the tool and support results from the visual core inspection.

consistent with the Cook Formation interpretation for the Oseberg area by Livbjerg and Mjøs (1989). Alternatively, these deposits may represent a tide-dominated delta lobe with a pronounced compensational stacking of deposits in local depocenters (Olariu et al., 2021; Wang et al., 2011; Straub et al., 2009). The distinction is challenging with the amount of available data. In the latter case, the lowermost portion of the Cook Formation could be interpreted as a distributary channel fill. The main limiting factor for plume behaviour in such coarse-grained sediments is the connectivity of the discrete sandstone bodies.

3.2. Depositional model

The sedimentary succession recognized from the wireline log trends and the core examination of the 31/5-7 well can be subdivided into three

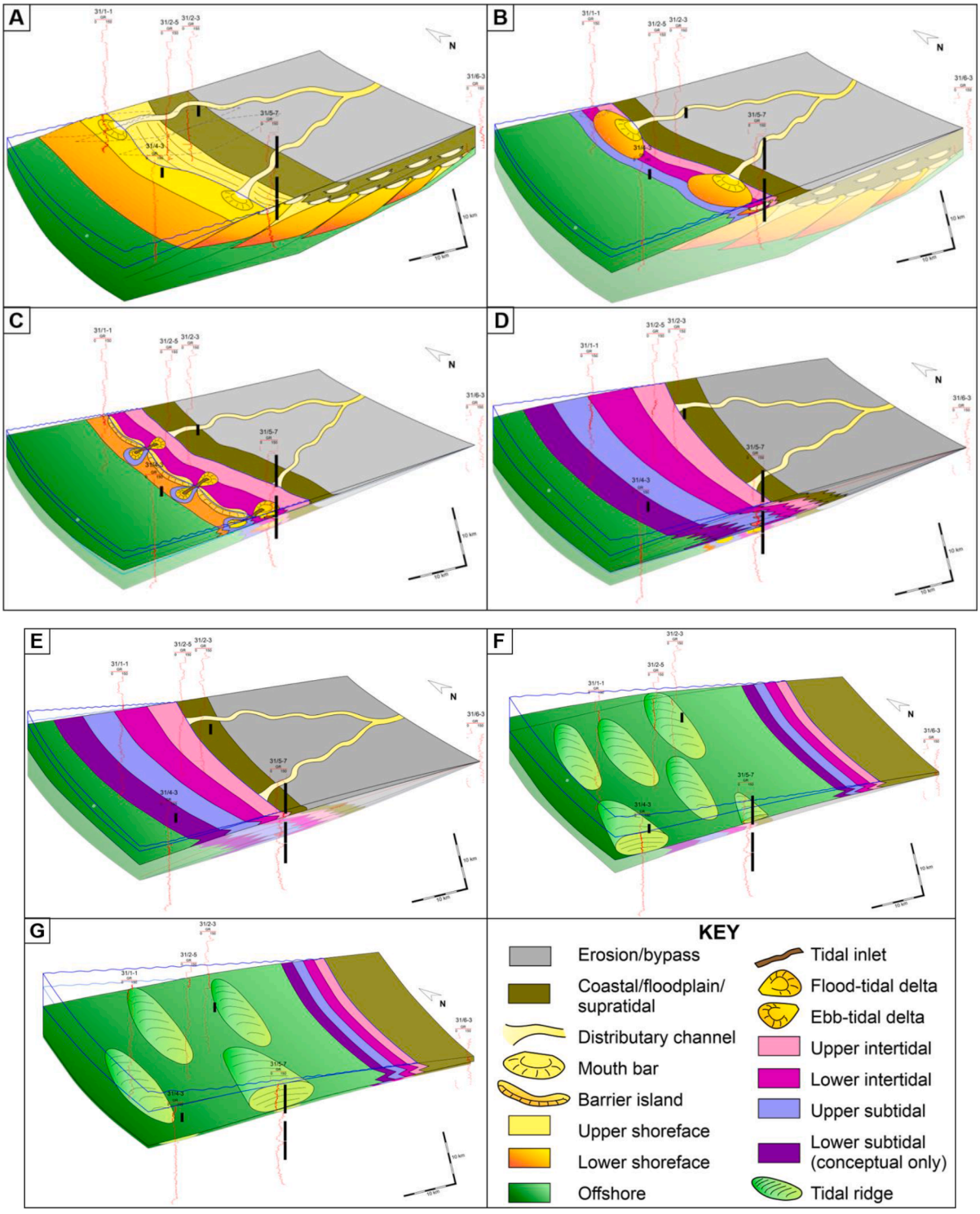

Fig. 8. Reconstructed depositional environment of the Johansen and Cook formations in the 31/5-7 well and selected offset wells. Vertical scale is exaggerated. Black rectangles: cored intervals. (A) Lower part of the Johansen Formation, wave-dominated delta/shoreface with distributaries (prograding). (B) Lower part of the Johansen Formation, interdistributary bay or tidal flat (aggrading). (C) Middle part of the Johansen Formation, barred coastline (transgressive). Landwards sediment transport direction is recorded by FMI data. (D) Upper part of the Johansen Formation, open-coast tidal flat (aggrading).

intervals expressing the depositional evolution (Fig. 8), from the base:

- Lower Johansen Formation (including the lower intertidal FA);
- Upper Johansen Formation and "Burton Formation-equivalent";
- Cook Formation

The Lower Johansen Formation encompasses the gradual transition from the underlying Amundsen Formation to the top of core no. 4, with a thickness of ca. 70 m (Fig. 2). It records the transition from inferred shallow-marine deposits below the cored intervals in 31/5-7 (lower shoreface and delta front) to coastal deposits (subaqueous distributary channel and mouth bar FA), and finally to paralic deposits (interdistributary bay or tidal flat of the lower intertidal flat FA), reflecting an overall progradational to aggradational trend (Fig. 8 A and B). This depositional pattern correlates well with the observed bell-shaped GR log trend (upward coarsening/cleaning then fining/dirtying), which is the typical signature of the Johansen Formation in the reference well 31/2-1 (Vollset and Doré, 1984) and in the other cored well 31/2-3 (Sundal et al., 2016) and matches with the typical signature of shallow-marine sandstones in wave-dominated systems (Hampson and Storms, 2003). Large-distance correlation to well 31/1-1 (27 km NW of Eos, Fig 1A) with a comparable log pattern also in the aggradational interval suggests high lateral persistence of the system, although with small-scale variability due to the mixing of processes and potentially local minor fluvial input. From FMI, the main sediment transport direction of the shallow-marine progradational deposits is towards the S-SW, compatible with a NE sediment source in the Sognefjord area in the Norwegian hinterland and with previously observed stratigraphic pinch out towards the S and W (Sundal et al., 2016). The transport direction is more variable in the paralic aggradational deposits (S, ENE, WNW, Fig. 9A, Appendix 5), reflecting a decrease in the depositional gradient and a higher variability of processes (tidal, wave and fluvial).

The middle interval (Upper Johansen Formation and "Burton Formation-equivalent") includes the deposits recorded in core no. 3 and the base of core no. 2, with a thickness of ca. 55 m. The base of this interval is the sharp contact between lower intertidal FA and inlet/flood tidal delta FA at the top of core no. 4. The lower part of the Upper Johansen Formation is interpreted as a short-lived transgression, with the development of a barred coastline and mixing of wave-and tide-processes. Tidal processes become predominant in the overlying interval with intercalations of upper subtidal FA and tidal channel FA (2734–2709 m core depth, Appendix 4). The GR log pattern in the overall interval is more erratic, but the fining-upwards trend at the top of core no. 3 culminating with the upper intertidal flat FA observed at the base of core no. 2 ("Burton Formation-equivalent") delineates an overall aggradational and progradational trend (Fig. 8 C and D). Correlation with offset wells is uncertain because of the lack of cores, and because of the inferred depositional setting, with high variability of processes and of sedimentary features. From FMI, the sediment transport direction of the transgressive sandstones (inlet/flood tidal delta FA) is landwards and displays a progressive rotation towards the N and NW in the aggradational and progradational part (Fig. 9A).

The upper interval (Cook Formation) is marked at the base by the possibly unconformable surface between upper intertidal FA ("Burton Formation-equivalent) and compound dune FA in the lowermost part of core no. 2. The Cook Formation in the Eos well is ca. 55 m thick and presents a fining upwards trend both from log and core, with thinning of stacked toeset/foreset couples (Fig. 7), expressing increasing tidal influence. The lateral extent of the tidal ridges or subaqueous delta front is in the order of tens of km^2 (Stride et al., 1982). Log patterns from offset wells in corresponding intervals show high variability, and discrete sandstone bodies cannot be correlated between wells distant more than 10 km. However, lateral ridge shift and storm reworking can provide large-scale sandstone connectivity. The sediment transport direction of the Cook Formation is predominantly towards the N and NW, sub-parallel to the inferred coastline configuration (Fig. 10B) (Churchill et al., 2017; Husmo et al., 2013), supporting the interpretation of tidal sand ridges rather than a tidal delta front.

Overall, the stratigraphic succession from the Lower through Upper Johansen, "Burton Formation-equivalent" and Cook formations is accommodated by a relative sea-level rise, with periodic coastal advancements and regressions, before culminating in a transgression and deposition of the marine shales of the Drake Formation. In the Eos well, the Drake Formation is 128 m thick, of which the lower 75 m are constituted by mudstones (Fig. 2B). Pressure measurements in the well strongly support the suitability of the Drake Formation as cap rock (Meneguolo et al., 2020). Additional characterization of the unit included rock mechanical testing and mineralogical composition and further confirmed that the Drake Formation would act as a robust top seal for the injection targets (Thompson et al., 2022, 2021; Meneguolo et al., 2021).

Fig. 8 Reconstructed depositional environment of the Johansen and Cook formations in the 31/5-7 well and selected offset wells. Vertical scale is exaggerated. Black rectangles: cored intervals. E) "Burton Formation-equivalent", open-coast tidal flat (prograding). F) and G) Cook Formation, tidal sand ridge (compound dune FA). An upwards decreasing energy trend and/or shallowing water development is inferred from the thinner toeset/foreset pairs and by the fining upwards trend. The Cook Formation deposits are then capped by the marine shales of the Drake Formation.

3.3. Property distributions

The three fining-upwards sequences identified in the Eos well (Fig. 3)

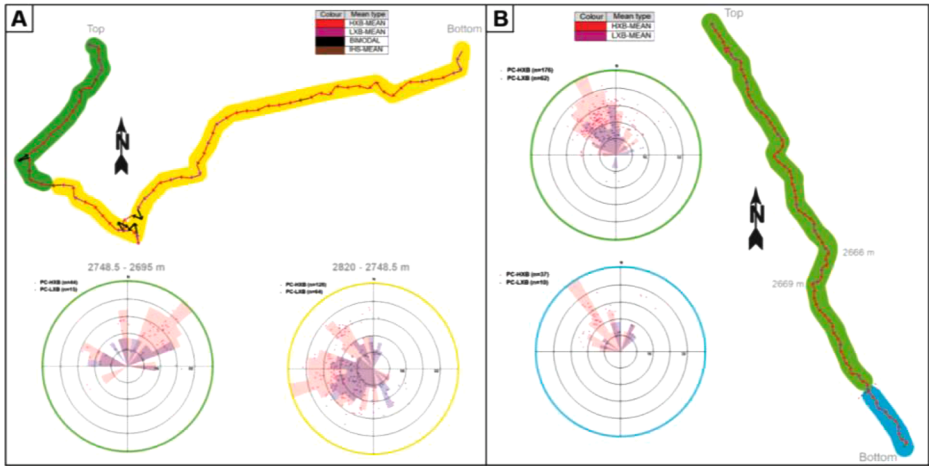

Fig. 9. Cross-set mean walkout plots from FMI, displayed as sequences of de-rotated sediment transport direction vectors. (A) Johansen Formation. A progressive rotation from a WSW-ly and SW-ly discharge (upper right corner) to a NW-ly discharge in the in the lower interval (yellow) can be observed. The central interval (green) displays fewer reliable measurements, directed towards the NW and NE, mostly from the lowermost part. (B) Cook Formation. A stable NNW-ly discharge is observed throughout the succession. Blue: basal 4.5 m, dominated by lithofacies Xco. Green: typical lithofacies array for the compound dune FA, with Xml, Xmh and secondarily Sm. No change in sediment transport direction can be observed between the two lithofacies groups. (For interpretation of the references to colour in this figure legend, the reader is referred to the web version of this article.)

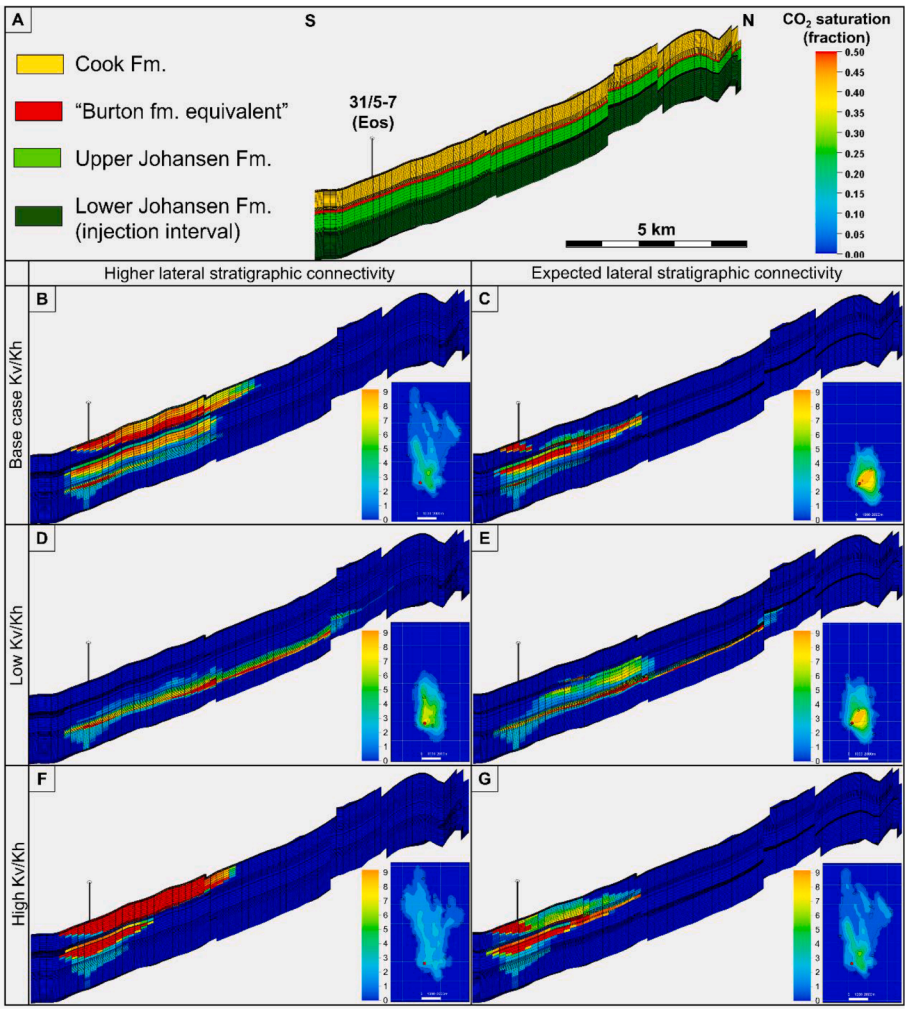

Fig. 10. Impact of heterogeneities in CO_2 behaviour after 30 years after injection start (25 years injection + 5 years post-injection), modelled as single sensitivities. Vertical exaggeration: 12 times. (A) S-N cross-section of the dynamic model grid across the Eos well with regions by formation. Cross sections are arranged by sensitivities on Kv/Kh (rows) and lateral stratigraphic connectivity (columns). For each scenario, a CO_2 height map is displayed, showing the geographical extent of the plume. (B) and (C) CO_2 is retained beneath the Lower intertidal FA and the "Burton Fm. equivalent" baffles and redistributed within both Cook and Johansen fms. (D) and (E) Higher lateral connectivity of Lower intertidal FA and "Burton Fm. equivalent" baffle combined with poor permeability restricts upwards CO_2 migration into the Cook Fm. and cause enhanced CO_2 travel in lower Johansen Fm. beneath the Lower intertidal FA baffle. (F) and (G) Reduced baffling of the poor permeability layers cause majority of CO_2 to migrate from the Johansen Fm. into the Cook Fm.

constitute the three main reservoir units included in the 3D reservoir model for the Aurora prospect: Lower and Upper Johansen and Cook formations respectively. Significant finer-grained intervals (thicker than 50 cm and potentially > 1 km^2 lateral extent) have been characterized and included separately in the property model in order to assess their baffling effect on fluid flow. Two such potential flow baffles are: 1) a 7 m thick heterolithic interval composed of the lower intertidal flat FA and capping the Lower Johansen Formation at 2748-2755 m (Fig. 8B), and 2) an 11 m-thick heterolithic interval corresponding to the upper intertidal flat FA ("Burton Fm. equivalent") between the Upper Johansen and Cook formations at 2696-2705 m (Fig. 8E). The top of the geomodel grid corresponds to the Drake Formation and represents the impermeable cap rock.

Consequently, three-dimensional grids were created for the three identified reservoir zones and the two potential baffling intervals, the lower intertidal flat FA (intra-Johansen) and the upper intertidal flat ("Burton Fm. Equivalent") (Table 2). Petrophysical evaluation of wireline logs calibrated to porosity and permeability measurements from core plugs constituted the input to the petrophysical model and are summarized in Table 2. A further calibration was performed based on the dynamic test result, which led to the application of 2,5-fold increase to the plug-calibrated petrophysical horizontal permeability log above a

Table 2
Overview of property ranges for the identified reservoir intervals (Lower and Upper Johansen, Lower and Upper Cook) and non-reservoir intervals (Lower intertidal flat FA and "Burton Formation equivalent") in the Eos well from plug-calibrated petrophysical log evaluation, and averages per zone in a representative area of the reservoir model (all cells reached by the plume at its largest extent). The Drake Formation is defined as impermeable seal. The Lower intertidal FA (upper part of the lower Johansen Fm.) includes discrete sandstone bodies which increase permeability. N/G: Net-to-Gross ratio. PHIT: total porosity. KLOGH: horizontal permeability. As the properties has been varied away from the well, the Eos properties may not be representative of the averages in the selected area.

Interval		Eos well logs calibrated to core plugs					Sampling from reservoir model		
		Gross (m)	Net (m)	N/G (m/m)	PHIT V/V	KLOGH mD	N/G (m/m)	PHIT V/V	KLOGH mD
	Drake Formation	127.9	0.0	0.0	-	-	-	-	-
3	Upper Cook	5.8	3.1	0.53	0.12 - 0.25	10 - 100	85	0.18	159
	Lower Cook	50.9	49.4	0.97	0.18 - 0.28	500 - 1000	1120	0.22	427
2	"Burton Fm. equivalent"	7.3	0.4	0.06	0.05 - 0.14	1 - 10	2	0.10	12
	Upper Johansen	51.6	44.9	0.87	0.12 - 0.28	100 - 200	420	0.23	245
1	Lower intertidal flat FA	11.7	11.5	0.98	0.08 - 0.15	10 - 100	490	0.24	113
	Lower Johansen	52.8	49.1	0.93	0.17 - 0.28	100 - 1000	1080	0.21	2234

400 mD threshold.

Because of the large distances to correlating wells and overall lack of core material for comparison, a new, regional facies modelling was not constructed based on the data addition from the Eos well (e.g. in the scales presented by Marjanac, 1995; Husmo et al.; 2003; Sundal et al., 2016 and Halland et al., 2011). Properties have been distributed stochastically with vertical increasing trend in the Lower and Upper Johansen and in the Lower Cook intervals, and with decreasing trend in the Lower intertidal flat FA, "Burton Fm. Equivalent" and Upper Cook intervals. Spatial property variations have been derived from the reconstructed proximal-distal depositional trends (Fig. 8) and approximated by lateral trends, while lateral connectivity of facies has been approximated by variogram length. A representative sample of the petrophysical properties in the geomodel for the expected Kv/Kh is shown on Table 2.

To establish well control in the proposed injection area has, however, been a crucial addition of information of local facies and properties for further evaluation of injectivity and migration paths (e.g. in the lower versus upper reservoir intervals). In previous fluid flow simulation models (e.g. Sundal *et al.*, 2015; Gassnova, 2012), porosity and permeability of the Johansen Fm. have been inferred from 3D seismic attributes and assigned porosity reductions with depth due to estimated diagenetic imprints. The range of estimated effective porosity was 7.3 - 31.4%, applied to only one flow unit (Sundal et al., 2015). The actual core observations and property measurements now available from the Eos well allowed reassessment of the Johansen and Cook formations in a local and regional context, constraining the geological model (Table 2) and reducing uncertainties by narrowing the property ranges and by refining the zonation and vertical trends..

Average porosity is similar in the Upper and Lower Johansen reservoir intervals, while permeability is significantly lower in the Upper Johansen unit, due to smaller average grain size and consequently smaller pore throats. The degree of heterogeneity (i.e. presence of lithofacies Sbs and Sbl with mm- to cm-scale mud drapes, Table 1 and Fig. 5C) is also higher in the Upper Johansen interval. These observations led to the selection of the Lower Johansen Formation as the injection interval, to maximize injectivity over time.

Within the Cook Formation, both the porosity and permeability decrease towards the top of the reservoir. A higher degree of heterogeneity is observed in the Upper Cook unit (i.e. grain-size variations in lithofacies Xmh and presence of mud-draped toesets, fluid muds and accretion surfaces in lithofacies Xml, Fig. 1; 6B). The non-reservoir units lower intertidal flat FA and the upper intertidal flat FA ("Burton Formation equivalent") constitute alternations of mud-rich, silty and sandy lamina, cm-thick and mm-thick respectively (Figs. 5A; 6A), determining repeated high permeability contrasts, but an overall low average value. Frequent, cm-thick sandstones lenses in the lower intertidal flat FA determine a slightly higher average permeability compared to the upper intertidal flat FA ("Burton Formation equivalent"), which presents a higher baffling potential than for the intra-Johansen flow baffle.

3.4. Single sensitivities

In order to address the effect of depositional features on CO_2 sequestration in the Storage Complex in EL001, vertical and lateral heterogeneities were tested as single sensitivities. The stratigraphic variability (lateral persistence of sandy intervals; presence and extent of lower intertidal flat FA and of "Burton Fm. equivalent") has been addressed in the property model with changes in variogram length as proxy of the lateral connectivity of the zones, while sedimentological heterogeneities have been approximated by the ratio between vertical and lateral permeability (Kv/Kh). A Kv/Kh range of 0.01 to 0.8 has been applied to all zones in addition to the vertical property trend, expect for the "Burton Fm. equivalent" which has been assigned a range of 0.01 to 0.1.

Two cases of lateral connectivity were tested: expected and higher. The effect of Kv/Kh variations was studied by defining a base (intermediate), a low and a high case. Comparisons between the different cases are shown in Fig. 10, with a 2-D S-N cross-section illustrating the plume development. It should be noted that the selected 2-D cross-section is not representative of the CO_2 distribution in the entire unit, however it captures the relative plume distribution between the units. The modelled faults are those identified with a throw from seismic interpretation, which are denser at a distance of 7 km from the injection well towards the N.

The impact of the different property scenarios has been quantified in terms of relative changes in volume stored in each unit after 30 years from injection start and is summarized as tornado charts in Fig. 11. The largest effects on volume occur for the higher lateral connectivity model combined with low Kv/Kh, causing CO_2 to be trapped in the Lower Johansen Formation and not reaching the Cook Formation (Fig. 10D; 11A and C). The most efficient CO_2 trapping is reached with the expected lateral connectivity model combined with high Kv/Kh, allowing storage in all three intervals (Figs. 10G; 11B and D). The expected Kv/Kh and lateral connectivity combination is marginally less effective, with a 13% decrease of stored CO_2 in the Johansen Formation and a corresponding increase in the Cook Formation (Figs. 10C; 11B).

Overall, the array of identified properties and heterogeneities indicate high likelihood for efficient plume redistribution and high sequestration potential in all cases.

4. Discussion

The new geological data set acquired from the 31/5-7 well represents the most complete record currently available from the Early Jurassic Dunlin Group. The increased knowledge of this unit has implications for both the understanding of the Early Jurassic stratigraphy in the central Horda Platform and for the suitability of the Aurora storage site for geological CO_2 sequestration. The local facies variation and degree of heterogeneity with implications for CO_2 injectivity and storage potential has been reassessed for the proposed storage reservoirs in the EL001 license; the Johansen and Cook formations, respectively.

4.1. Stratigraphic framework and depositional environment in the EL001 area

The core, borehole image log and biostratigraphic datasets from the Eos well enabled the reconstruction of the sedimentary environment and stratigraphic development of the Dunlin Group. The depositional setting of the Johansen Formation is marginal- marine (coastal to paralic) and wave-dominated, as previously proposed by Sundal et al. (2016). The reconstructed location of the well is in a more distal position than offset well 31/2-3, in the same depositional belt as offset well 31/1-1 which is also interpreted to record the aggradation at the top of the Lower Johansen interval (Fig. 8).

Biostratigraphic information has been crucial for the interpretation of the mud-dominated heterolithic interval above the Johansen Formation (upper intertidal flat FA) as paralic (Fig. 3). The interpretation of brackish conditions and tidal influence is in accordance with the observations of Bell et al. (1984), for wells in the 31/6-block, to the NE of EL001. This also corresponds to lagoonal and back barrier facies previously assigned to eastern parts of the Upper Johansen Formation (Sundal et al., 2016). However, Bell (1984) extended the interpretation of brackish conditions in time and space, also based on biostratigraphy, excluding a marine incursion between the Johansen and Cook formations. The mudstone interval often separating the Johansen and Cook formations has previously been interpreted in the Troll West area as a marine shale representing a flooding episode and comprising a Maximum Flooding Surface marking the turning point before renewed coastal progradation (Parkinson and Hines, 1995; Marjanac and Steel, 1995; Sundal et al., 2016), without an aggradational interval. These interpretations were, however, based only on well logs and cuttings.

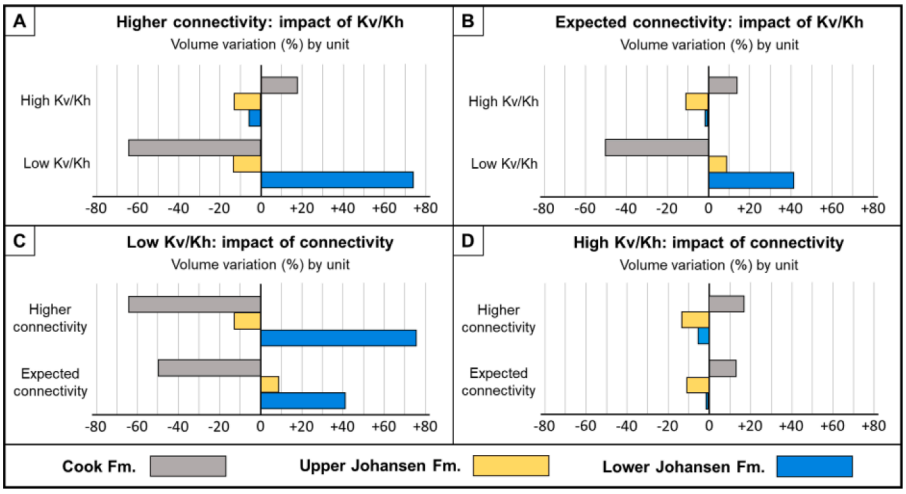

Fig. 11. Tornado charts of the relative variation in free CO_2 by unit, after 30 years after injection start. (A) Effect of Kv/Kh in the higher lateral connectivity model. (B) Effect of Kv/Kh in the expected lateral connectivity model. (C) Effect of lateral connectivity in the low Kv/Kh model. (D) Effect of lateral connectivity in the high Kv/Kh model.

Biostratigraphic evidence from the Eos well (dominant fresh-to brackish-water indicators such as Acritarcs and Dinoflagellate cists, Fig. 3) supports instead a shallower depositional setting for this interval, as the culmination of an overall basinwards facies shift in a paralic, tidally-modulated environment.

The characteristics of the muddy upper intertidal flat FA in the 31/5-7 well are distinct in comparison to both the over- and underlying sandy units in the Cook and Johansen formations (compound dunes and upper subtidal flat FA, respectively), and its occurrence is inferred only in the north-western area (Fig. 1A). For these reasons, this interval has been attributed a separate stratigraphic designation as "Burton Formation-equivalent" (correlative marginal deposits lateral to the basinal Burton Formation mudstones, Vollset and Doré, 1984). Alternatively, the Johansen Formation lithostratigraphic top boundary could be redefined at the contact between the lower intertidal flat FA and the inlet/flood tidal delta FA (Fig. 8B; C).

The Cook Formation in the 31/5-7 well is interpreted to be composed of one unit, formed by tidally dominated, laterally shifting compound dunes or tidal ridges in a shallow shelf, and directly overlain by the marine shales of the Drake Formation (Fig. 3). The observed increase of tidal processes in the Cook Formation is compatible with tidal amplification because of shelf enlargement (Darlymple, 2010; Darlymple and Choi, 2007) because of relative sea-level rise. The increase of tidal influence in the Cook Formation sandstones determines a decrease in sediment sorting (Table 1), and an increase in the frequency of mudstone interlayers, particularly in the upper part of the unit.

The bipartite subdivision of the Cook Formation (wave-dominated interval followed by tidal-dominated deposits, crf. Dreyer and Wiig, 1995; Folkestad et al., 2012; or tidal deposits underlying a wave-dominated unit, crf. Churchill et al., 2017) is not recognized in the Eos well, and regional correlation is uncertain. The absence of a wave-dominated interval could be attributed either to condensation below the Drake Formation, or to erosion by the subsequent tidal succession. An alternative lithostratigraphic subdivision of the sedimentary succession in the 31/5-7 well could attribute the central, paralic interval to the Cook Formation. In this case, the inferred barred coastline with mixing of wave-and tide-processes (Fig. 8C) could correspond to the wave-dominated lower part of the Cook Formation as in Dreyer and Wiig (1995) and Folkestad et al. (2012). The upper intertidal flat FA below the compound dune FA would not fit the stratigraphic position of the Burton Formation and would simply represent the shallowest recorded portion of the paralic interval. This option is considered less likely because of the overall gradual transition from the coastal to the paralic deposits (Lower to Upper Johansen Formation), while the most prominent stratigraphic break occurs between the upper intertidal flat FA and the compound dune FA, justifying the lithostratigraphic attribution of the tidal ridges to the Cook Formation.

The stratigraphic development of the Dunlin Group in the Horda Platform could be refined with the dataset acquired in the Eos well, Nevertheless, the limited information and large distance (> 10 km) of the nearest offset wells reduces the confidence on the vertical and lateral connectivity as well as on property distribution of the reservoir units, which are therefore tested in various property scenarios of the CO_2 flow model.

4.2. *Lateral connectivity in reservoir units*

High quality reservoirs suitable for CO_2 storage must have good injectivity and high storage potential, which depend on *in-situ* thermodynamic conditions and geological reservoir properties (Halland et al., 2011; Bachu, 2003). The reservoir sweep may be larger in more heterogeneous reservoirs, increasing storage efficiency and security (Hovorka et al., 2004). In sloping aquifers (Fig. 1B), plume migration may be enhanced or retarded based on the relative orientations of structural dip, faults, sedimentary (and diagenetic) property trends and the distribution of flow baffles (Andersen and Sundal, 2021; Olivarius et al., 2019; Sundal et al., 2015).

The Storage Complex interval comprises sandy facies intervals in both the Johansen and Cook formations, roughly summing up to a total thickness of reservoir grade sand in the order of 120 m in the Eos near-well area (Fig. 1, Table 2). CO_2 injection is planned in the Lower Johansen Formation (Figs. 5 and 8A and B), through an inclined side-track well, and buoyant CO_2 is predicted to migrate upwards and NNW-wards due to the structural dip (Figs. 1B and 11). In the shallow-to marginal- marine deposits of the injection interval, high sandstone connectivity is likely. Directional permeability anisotropy would be expected between depositional strike (Ky) and dip (Kx) orientations, with higher permeability parallel with the NNW-SSE paleo coastline (Ky), facilitating CO_2 migration through porous shoreface and mouth bar deposits (Fig. 8A). In the Lower Johansen Fm., lateral connectivity and overall high porosity and permeability may facilitate CO_2 migration in the lower reservoir unit, potentially enhancing sweep (Fig. 10B; C). In the Upper Johansen unit (Fig. 8C), higher variability of sandstone transport directions (with a recorded eastward component, Fig. 3) and the interpreted smaller-scale bodies implies that CO_2 could be funnelled also towards the west within flood delta deposits and north into barrier

bars/spit deposits (facies model in Sundal *et al.*, 2016). The same NNW-SSE coastline orientation and high connectivity parallel with the assumed preferred migration along the northwards structural dip is inferred for the upper part of the Upper Johansen unit (Fig. 8D). The average permeability (Kx, Ky) is, however, lower in these heterogeneous deposits interpreted as a paralic environment with tidal processes (Table 2). Although still reservoir-grade sandstones, the higher mudstone content and the smaller spatial dimensions of the dominant discrete heterogeneities suggest even higher reservoir sweep potential (Fig. 10B and C), which would enhance the effect of physical and chemical trapping (Sundal et al., 2015; Sundal and Hellevang, 2019). Overall, high lateral connectivity throughout the Johansen Formation interval is supported by the interpretation of the results from the drill stem test performed in Eos, showing no indications of compartmentalization and high pressure dissipation capacity in the estimated investigation radius of 2 to 3 km (Meneguolo et al., 2020). This indicates that draping mud-layers and carbonate cemented zones are not continuous and/or tight enough to cause problems with near-well pressure build-up, although they still may direct buoyant fluids. High permeability and good connectivity are the main factors allowing the injection of the Phase one volumes (37.5 Mt) without reaching the Bottom Hole Pressure constraint in the geomodel output.

The tidal ridges of the Cook Formation (Fig. 8F and G) are discrete (>10 m thickness, >100 m width, >1000 m length; Swift, 1975), NNW-ESE elongated features, with down-lapping geometries towards the E and W, respectively. Sedimentary infill between sand ridges is in parts redistributed sand, and in parts marine mud (Drake Formation). Variations in connectivity have been tested by modifying variogram lengths (Fig. 10B; C), resulting in a marginal difference in stored CO_2 for high Kv/Kh ratios (Fig. 11D). The ridges must be mapped out in detail to describe their average orientation relative to the structural dip and faults, to evaluate funnelling of CO_2 towards the NNW vs. trapping effects (Andersen and Sundal, 2021).

4.3. Effect of vertical flow baffles/barriers

Silty or very fine interlayers in otherwise sandy reservoirs will retard upwards migration and spread the CO_2 plume in the injection area (Flett et al., 2007; Frykman et al., 2009). In the Eos well, most inter-layers are thin (Figs. 4 and 5A) and unlikely to cause more than 1/10 vertical permeability anisotropy in the reservoir sand interval, allowing CO_2 to migrate towards the top of the primary unit within a relatively short time frame (Alfnes et al., 2004; Sundal et al., 2015) (Fig. 11D). The muddy lower intertidal FA at 2749–2754 m (Fig. 5A) is likely, however, to cause significant retardation and local spreading of the plume beneath it (Fig. 10D; E), causing enhanced trapping in the Lower Johansen Formation (Fig. 11C). The discrete sandstone bodies identified in the interval above (Fig. 8C) may however disrupt the continuity of the lower intertidal FA and cause an increase the vertical connectivity (increase in Kv/Kh), thus allowing for vertical CO_2 migration (Fig.11F; G; 12D).

The mud-dominated heterolithic interval above the Johansen Formation (upper intertidal flat FA) has previously been interpreted as a marine shale in the Troll West area (Parkinson and Hines, 1995; Marjanac and Steel, 1997; Sundal et al., 2016), with the implication that the layer could be extensive. Previous simulations (Sundal et al., 2015) including a muddy interval (Amundsen Formation, PHIE < 6%) between the Johansen and Cook formations predicted CO_2 to reach the top of the secondary reservoir within 50 years. However, the current interpretation of the upper intertidal flat FA ("Burton-Formation equivalent") implies that the unit is sandier, more heterogeneous, and not necessarily as laterally continuous compared as stated in previous interpretations, and thus likely to slightly retard, but not severely inhibit vertical CO_2 migration between Johansen and Cook formations (Figs. 10B; C, 11A; B).

4.4. Effect of small-scale sedimentological heterogeneities

In the shallow-to marginal marine Johansen Formation, inclined flow baffles such as mud-drapes and carbonate-cemented layers are expected to reduce E-W reservoir communication, and/or cause some funnelling towards the east, from toe sets to top sets (e.g. Flett et al., 2007). Carbonate cemented zones, varying in thickness (< 0.4–2 m), are observed (from petrophysical well logs) in all wells penetrating the Johansen Formation (Sundal et al., 2016), and these are also recognized in Eos (Fig. 5C, Appendix 4; 5). It has been a concern whether these would represent laterally extensive layers, which have been known to pose a challenge in some reservoirs (Bjørkum and Walderhaug, 1990; Gibbons et al., 1993). However, most calcite-cemented intervals observed in core appear as rounded with irregular margins, indicative of large concretions rather than continuous layers. They are thus interpreted as very local features, and although they may appear more frequent in horizons due to carbonate sourced from mollusc beds etc., they are not thought to pose any significant effect on fluid flow.

From thin section petrography in new samples deeper than 2700 m, it is evident that reservoir deterioration due to quartz cementation and other diagenetic processes is minor (Fig. 12). Textures and reactive mineral assemblies are comparable to previous studies (Sundal and Hellevang, 2019), providing permeable sandstone with significant potential for immobilizing CO_2 through residual, dissolution and mineral trapping. Estimated moderate kinetic reaction rates improve storage security without compromising injectivity (Sundal et al., 2021).

The tidally influenced compound dune FA in the Cook Formation displays thin silty/muddy toesets and intervals between individual dunes sets presenting high permeability contrasts (Fig. 6). Small-scale heterogeneities (mm-dm), such as cross-lamination and preferred grain orientation, will also contribute to vertical permeability reduction (Ringrose et al., 1993). However, the N-NW migrating cross-stratified sediments in the Eos well cause these heterogeneities to be oriented orthogonally to the assumed direction of CO_2 migration, thus enhancing plume spreading. Within the overall very sandy, but heterogeneous, compound dune FA, buoyant migration is likely very efficient, while residual trapping and dissolution potential is also high as these sequestration mechanisms are pore-size dependent (Bachu and Bennion, 2008) and enhanced by properties contrasts (Harris et al., 2021; Kim et al., 2021).

4.5. Suitability of shallow-marine sandstones for CO_2 storage

A coastal, wave-dominated depositional setting similar to that of the Johansen Formation is interpreted for the current injection unit of the Snøvhit CO_2 storage site (Late Pliensbachian to Bajocian Stø Formation), and of the Sleipner storage site (Middle to Late Miocene Utsira Formation). The Johansen Formation in well 31/5-7 presents comparable thickness to the Stø Formation, but slightly higher average properties (porosity above 20% for the Johansen Formation; between 15 and 20% in the Stø Formation: Table 2, Halland et al., 2011). The higher properties in the Utsira Formation (30-40% porosity, 2D permeability, Zweigel et al., 2004) can be attributed to the shallower burial depth. Mud removal by wave action (increased sorting, Table 1) and sediment transport by longshore current over large areas are optimal conditions for high permeability sandstones with connectivity over large distance.

A lower degree of lateral connectivity can be inferred for the Cook Formation, for which discrete sandstone bodies in a muddy background are interpreted. This lithological and permeability contrast could provide local traps and pressure compartments, analogously to the fluvial Tubåen injection unit of the Snøvhit storage site (Shi et al., 2013). However, individual sand bodies of the lower Cook Formation are likely to allow for pressure connection to the underlying, highly connected reservoir units where injection will occur, constituting and upside for storage.

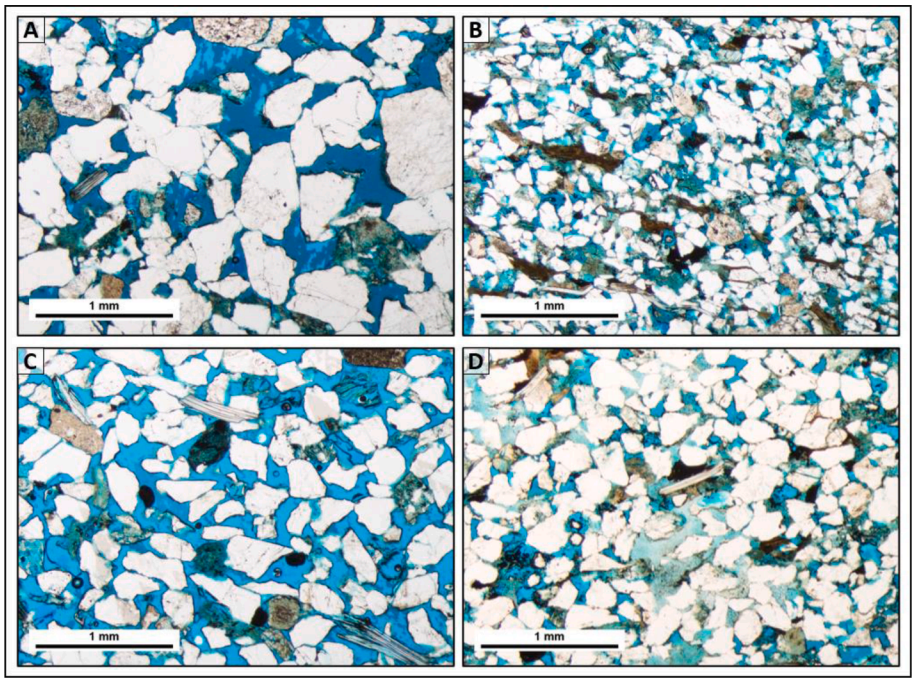

Fig. 12. Petrography of selected samples from the sandy facies of the Dunlin Group in well 31/5-7. Sample location in Fig. 3. (A) Mouth bar FA, 2771.70 m MD, Johansen Formation. Well-sorted, lower coarse-grained sandstone; Qtz/Fsp 4.0; Porosity 15.8%; (B) Subaqueous distributary channel FA, 2757.32 m MD, Johansen Formation. Well-sorted, upper-fine-grained sandstone; Qtz/Fsp 3.6; Porosity 16.3%; (C) Inlet/flood tidal delta FA, 2741.83 m MD, Johansen Formation. Well-sorted, lower medium-grained sandstone; Qtz/Fsp 6.3; Porosity 25.3%; (D) Compound dune FA, 2679.45 m MD, Cook Formation. Well-sorted, upper medium-grained sandstone; Qtz/Fsp 5.0; Porosity 23.5%.

5. Conclusions

The geological information acquired in the 31/5-7 well represent the most complete dataset currently available on the Early Jurassic Dunlin Group. The well has been crucial to increase understanding of both the Early Jurassic stratigraphy in the central Horda Platform and to assess the suitability of the Aurora prospect for geological CO_2 storage.

The intended storage units of the Dunlin Group (Johansen and Cook formations) encompass a marginal- to shallow-marine succession, shifting from mixed wave-tide-and-river-influenced high-energy coastal deposits (shoreface intersected by distributaries) to a paralic low-energy, fine-grained unit (interdistributary bay), followed by a short-lived barred coastline and by a prograding open-coast tidal flat. This is possibly unconformably overlain by shallow-marine, high-energy tidally dominated deposits (tidal ridges).

These three intervals are all fining-upwards and delineate an overall relative sea-level rise. Main identified factors affecting plume behaviour are lateral connectivity and vertical baffles, investigated through a 3D geological static and a dynamic fluid flow model. The measured excellent reservoir properties (100-1000s mD) in the Eos well are comparable to those from the shallow marine Utsira and Stø formations storage units, where high injectivity has been successfully demonstrated through the Sleipner and Snøvhit schemes for CCS.

The modelled scenarios for reservoir connectivity and property variability resulted in a high storage resource potential. The repeated fining-upwards trends and the identified meso-scale vertical flow baffles constitute the crucial factor for plume redistribution and efficient CO_2 storage, without compromising the pressure dissipation capacity.

The observations from well 31/5-7 (Eos) represent ideal pre-requisites for geological storage assessment. Evaluation results indicate enhanced CO_2 plume redistribution potential and available storage resource for the ambition of the first industrial-scale CCS project in Norway and worldwide.

Funding

This research received to specific grant from any funding agency in the public, commercial or non-for-profit sectors.

Data availability

Datasets from the 31/5-7 well utilized in this study are individually available in full resolution in raw and other formats via www.data.equinor.com

CRediT authorship contribution statement

Renata Meneguolo: Conceptualization, Project administration, Writing – original draft. **Anja Sundal:** Conceptualization, Investigation, Writing – original draft. **Allard W. Martinius:** Conceptualization, Investigation, Validation, Writing – review & editing. **Zbynek Veselovsky:** Methodology, Validation, Writing – original draft. **Alex Cullum:** Methodology, Validation, Writing – review & editing. **Elvira Milovanova:** Methodology, Validation, Writing – review & editing.

Declaration of Competing Interest

The authors declare that they have no known competing financial interests or personal relationships that could have appeared to influence the work reported in this paper.

Acknowledgments

The authors wish to thank the Northern Lights partners Equinor, Shell and Total Energies for challenging and fruitful discussion, and the members of the subsurface team for the support, patience, and cooperation. Particularly, Herre Bartlema, Kim Bye Bruun, Silvia Kassold, Kevin J. Keogh, François Lafont, Anne Lesueur, Rune Osland and Mark Wood are gratefully acknowledged for the thorough manuscript revision and improvement suggestions.

Supplementary materials

Supplementary material associated with this article can be found, in the online version, at doi:10.1016/j.ijggc.2022.103723.

References

Alfnes, E., Kinzelbach, W., Aagaard, P., 2004. Investigation of hydrogeologic processes in a dipping layer structure: 1. The flow barrier effect. J. Contam. Hydrol. 69 (3-4), 157–172.

Amer, A., Glascock, M., Schwalbach, J., Khan, M., 2011. Applied borehole image analysis in complex sedimentological and structural setting: a single well case study, California. In: SPE Annual Technical Conference and Exhibition 2011, 8th-10th October. Society of Petroleum Engineers, Colorado, USA.

Andersen, O., Sundal, A., 2021. Estimating caprock impact on CO_2 migration in the gassum formation using 2d seismic line data. Transp. Porous Media 138, 459–487.

Bachu, S., 2003. Screening and ranking of sedimentary basins for sequestration of CO_2 in geological media in response to climate change. Environ. Geol. 44 (3), 277–289.

Bachu, S., Bennion, B., 2008. Effects of *in-situ* conditions on relative permeability characteristics of CO_2-brine systems. Environ. Geol. 54 (8), 1707–1722.

Bell, D.G., Bjærke, T., Skarbø, O., 1984. Biostratigraphy Kerogen Analysis. Stratlab. for Statoil. (Report). Available online: 127_03_31_6_6_Biostratigraphy_Kerogen_Analysis.pdf (npd.no).

Bell, R.E., Jackson, C.A.L., Whipp, P.S., Clements, B., 2014. Strain migration during multiphase extension: observations from the northern North Sea. Tectonics 33 (10), 1936–1963.

Bhattacharya, J.P., Giosan, L., 2003. Wave-influenced deltas: geomorphological implications for facies reconstruction. Sedimentology 50, 187–210.

Bjørkum, P.A., Walderhaug, O., Buller, A.T., Berg, E., Hjelmeland, O., Kleppe, J., Trosæter, O., Aasen, J.O., 1990. Lateral extent of calcite-cemented layers in shallow marine sandstones. In: Second International Conference on the North Sea Oil and Gas Reservoirs. University of Trondheim, The Norwegian Institute of Technology. London, Graham & Trotman, pp. 333–336.

Cohen, K.M., Finney, S.C., Gibbard, P.L., Fan, J.X., 2013. The ICS international chronostratigraphic chart. Episodes 36 (3), 199–204.

Charnock, M. A., Kristiansen, I. L., Ryseth, A., and Fenton, J. P. G., 2001. In: Martinsen O. J. and Dreyer T. (Eds) Sedimentary Environments Offshore Norway - Palaeozoic to Recent. NPF Special Publication, 10, 145-174.

Churchill, J. M., Poole, M. T., Skarpeid, S. S., and Wakefield, M. I., 2017. Stratigraphic architecture of the Knarr Field, Norwegian North Sea: sedimentology and biostratigraphy of an evolving tide- to wave-dominated shoreline system. In: Hampson, G. J., Reynolds, A. D., Kostic, B. and Wells, M. R. (Eds) Sedimentology of Paralic Reservoirs: Recent Advances. Geological Society, London, Special Publications, 444, 35-58.

Dalrymple, R.W., Choi, K., 2007. Morphologic facies trends through the fluvial-marine transition in tide-dominated depositional systems: a schematic framework for environmental and sequence stratigraphic interpretation. Earth Sci. Rev. 81, 135–174.

Dalrymple, R. W., 2010. Tidal depositional systems. In: James, N., Dalrymple, R. (Eds.), Facies Models 4. Geol. Ass. Can., St. John's, Geotext 6, 201–231.

Dashtgard, S.E., 2011. Linking invertebrate burrow distributions (neoichnology) to physicochemical stresses on a sandy tidal flat: implications for the rock record. Sedimentology 58, 1303–1325.

Deng, C., Fossen, H., Gawthorpe, R.L., Rotevatn, A., Jackson, C.A.-L., Fazlikhani, H., 2017. Influence of fault reactivation during multiphase rifting: The Oseberg area, northern North Sea rift. Mar. Pet. Geol. 86, 1252–1272.

Dominguez, J. M. L., 1996. The São Francisco strandplain: a paradigm for wave-dominated deltas? In: De Batist, M. and Jacobs, P. (Eds) Geology of Siliciclastic Shelf Seas, Geological Society Special Publication 117, 217-231.

Donselaar, M.E., Schmidt, J.M., 2005. Integration of outcrop and borehole image logs for high-resolution facies interpretation: example from a fluvial fan in the Ebro Basin, Spain. Sedimentology 52, 1021–1042.

Dreyer, T., and Wiig, M., 1995. Reservoir architecture of the Cook formation on the Gullfaks field based on sequence stratigraphic concepts. In: Steel, R. J., Felt, V. L., Johannessen E. P., and Mathieu C. (Eds.) Sequence stratigraphy on the northwest European margin. Norwegian Petroleum Society Special Publication, 5, 109-142.

Duffy, O.B., Bell, R.E., Jackson, C.A.-L., Gawthorpe, R.L., Whipp, P.S., 2015. Fault growth and interactions in a multiphase rift fault network: Horda Platform, Norwegian North Sea. J. Struct. Geol. 80, 99–119.

Flett, M., Gurton, R., Weir, G., 2007. Heterogeneous saline formations for carbon dioxide disposal: impact of varying heterogeneity on containment and trapping. J. Pet. Sci. Eng. 57 (1–2), 106–118.

Folkestad, A., Veselovsky, Z., Roberts, P., 2012. Utilising borehole image logs to interpret delta to estuarine system: a case study of the subsurface Lower Jurassic Cook Formation in the Norwegian northern North Sea. Mar. Pet. Geol. 29, 255–275.

Frykman, P., Bech, N., Sørensen, A.T., Nielsen, L.H., Nielsen, C.M., Kristensen, L., Bidstrup, T., 2009. Geological modeling and dynamic flow analysis as initial site investigation for large-scale CO_2 injection at the Vedsted structure, NW Denmark. Energy Procedia 1, 2975–2982.

Færseth, R., 1996. Interaction of Permo-Triassic and Jurassic extensional fault-blocks during the development of the northern North Sea. J. Geol. Soc. 153, 931–944.

Gassnova, 2012. In: Andfossen, P. O., Horntvedt, L., Ravn, T., Rørvik, K.L., Diesen, M., Keaney, G., Torgersen, T.A., Vetaas, M.V., Erichsen, E., Mohr, J. (Eds.), Geological Storage of CO_2 from Mongstad. Interim Report Johansen Formation. Report TL02-GTL-Z-RA-0001.

Gibbons, K., Hellem, T., Kjemperud, A., Nio, S.D., Vebenstad, K., 1993. Sequence Architecture, Facies Development and Carbonate-Cemented Horizons in the Troll Field Reservoir, Offshore Norway, 69. Geological Society, London, Special Publications, pp. 1–31.

Gingras, M.K., MacEachern, J.A., Dashtgard, S.E., 2012. The potential of trace fossils as tidal indicators in bays and estuaries. Sediment. Geol. 279, 97–106.

Gradstein, F.M., Anthonissen, E., Brunstad, H., Charnock, M., Hammer, Ø., Hellem, T., Lervik, K.S., 2010. Norwegian Offshore Stratigraphic Lexicon (NORLEX). Newslett. Stratigr. 44 (1), 73–86. https://doi.org/10.1127/0078-0421/2010/0005.

Halland, E.K., Tjelta Johansen, W., Riis, F., 2011. CO_2 Storage Atlas, Norwegian North Sea. Norwegian Petroleum Directorate, Stavanger, Norway.

Hallam, A., 2001. A review of the broad pattern of Jurassic sea-level changes and their possible causes in the light of current knowledge. Palaeogeogr. Palaeoclimatol. Palaeoecol. 167 (1-2), 23–37.

Hampson, G.J., Storms, J.E.A., 2003. Geomorphological and sequence stratigraphic variability in wave-dominated, shoreface-shelf parasequences. Sedimentology 50, 667–701.

Harris, C., Jackson, S.J., Benham, G.P., Krevor, S., Muggeridge, A.H., 2021. The impact of heterogeneity on the capillary trapping of CO_2 in the captain sandstones. Int. J. Greensh. Gas Control 112, 103511.

Hertweck, G., Werhrmann, A., Liebezeit, G., Steffens, M., 2005. lchnofabric zonation in modern tidal flats: palaeoenvironmental and palaeotrophic implications. Senckenbergiana Maritima 35 (2), 189–201.

Hoecker, C., Eastwood, K.M., Herweijer, J.C., Adams, J.T., 1990. Use of dipmeter data in clastic sedimentological studies. Bull. Am. Assoc. Petrol. Geol. 74, 105–118.

Hovorka, S.D., Doughty, C., Benson, S.M., Pruess, K., Knox, P.R., 2004. The Impact of Geological Heterogeneity on CO_2 Storage in Brine Formations: A Case Study from the Texas Gulf Coast, 233. Geological Society, London, Special Publications, pp. 147–163.

Husmo, T., Hamar, G., Høiland, O., Johannesen, E. P., Rømuld, A., Spencer, A., and Titterton, R., 2003. Lower and middle Jurassic. In: Evans, D., Graham, C., Armour, A., and Bathurst, P. (Eds) The Millennium Atlas: Petroleum Geology of the Central and Northern North Sea. The Geological Society of London, United Kingdom, 129-155.

Kim, K.-Y., Kim, M., Oh, J., 2021. Core-scale investigation of the effect of heterogeneity on the dynamics of residual and dissolution trapping of carbon dioxide. J. Hydrol. 596, 126109.

Livbjerg, F., and Mjøs, R., 1989. The Cook Formation, an offshore sand ridge in the Oseberg area, northern North Sea. In: Collinson, J. D. (Ed.) Correlation in Hydrocarbon Exploration. Norwegian Petroleum Society, Graham and Trotman, London, UK, 299-312.

Marjanac, T., 1995. Architecture and sequence stratigraphic perspectives of the Dunlin Group formations and proposal for new type- and reference-wells. In: Steel, R.J., Felt, V.L., Johannessen, E.P., and Mathieu, C. (Eds.) Sequence stratigraphy on the northwest European margin. Norwegian Petroleum Society Special Publication, 5, 143-165.

Marjanac, T., Steel, R.J., 1997. Dunlin Group Sequence stratigraphy in the northern North Sea: a model for cook sandstone deposition. Am. Assoc. Pet. Geol. Bull. 81 (2), 276–292.

Meneguolo, R., Thompson, N.D., Sundal, A., Hellevang, H., 2021. Multi-scale cap rock assessment for CO_2 storage, insights from the Northern Lights project (Norwegian Continental Shelf). Basin and Petroleum System modeling: Best Practices, Challenges and New Techniques 2021. The Geological Society. London, and Virtual, 30th September.

Meneguolo, R., Målbakken, T., Galvani, L., Kassold, S., Vazquez Anzola, D.A., 2020. Subsurface contribution to the Northern Lights CO_2 storage project sanction: Planning for success in an unexplored license. In: SPE Carbon Capture Utilisation and Storage Conference 2020, Virtual Event, 26th - 29th October.

NPD – Norwegian Oil Directorate, 2019 Tildeling av utnyttelsestillatelse for lagring av CO_2 - Oljedirektoratet (npd.no).

Norwegian Government, 2020 Langskip –79/5000 A project for CO_2 management that includes capture, transport and storage of CO_2 (regjeringen.no).

Odinsen, T., Reemst, P., Van Der Beek, P., Faleide, J.I., Gabrielsen, R.H., 2000. Permo-Triassic and Jurassic extension in the northern North Sea: results from tectonostratigraphic forward modelling, 167. Geological Society, London, Special Publications, pp. 83–103.

Olariu, M.I., Olariu, C., Steel, R.J., Darlymple, R.W., Martinius, A.W., 2012. Anatomy of a laterally migrating tidal bar in front of a delta system: esdolomada Member, Roda Formation, Tremp-Graus Basin, Spain. Sedimentology 59, 356–378.

Olariu, C., Steel, R.J., Dalrymple, R.W., Gingras, M.K., 2021. Tidal dunes versus tidal bars: the sedimentological and architectural characteristics of compound dunes in a tidal seaway, the lower Baronia Sandstone (Lower Eocene), Ager Basin, Spain. Sediment. Geol. 279, 134–155.

Olivarius, M., Sundal, A., Weibel, R., Gregersen, U., Baig, I., Thomsen, T.B., Kristensen, L., Hellevang, H., Nielsen, L.H., 2019. Provenance and Sediment Maturity as Sequestration Controls on Potential CO_2 Mineral of the Gassum Formation in the Skagerrak. Front. Earth Sci. Sedimentol. Soc. 7 (312), 1–23.

Parkinson, D. N., and Hines F. M., 1995. The Lower Jurassic of the North Viking Graben in the context of western European Lower Jurassic stratigraphy. In: Steel, R.J., Felt, V.L., Johannessen E.P., and Mathieu C. (Eds.) Sequence stratigraphy on the northwest European margin. Norwegian Petroleum Society Special Publication, 5, 97-107.

Phillips, T.B., Fazlikhani, H., Gawthorpe, R.L., Fossen, H., Jackson, C.A.L., Bell, R.E., Faleide, J.I., Rotevatn, A., 2019. The influence of structural inheritance and multiphase extension on rift development, the northern North Sea. Tectonics 38 (12), 4099–4126.

Ravnås, R., Steel, R.J., 1998. Architecture of marine rift-basin successions. Am. Assoc. Petrol. Geol. Bull. 82, 110–146.

Ringrose, P.S., Sorbie, K.S., Corbett, P.W.M., Jensen, J.L., 1993. Immiscible flow behaviour in laminated and cross-bedded sandstones. J. Pet. Sci. Eng. 9 (2), 103–124.

Schlumberger, 2021. ECLIPSE Technical Description.

Shi, J.Q., Imrie, C., Sinayuc, C., Durucan, S., Korre, A., Eiken, O., 2013. Snøhvit CO_2 storage project: assessment of CO_2 injection performance through history matching of the injection well pressure over a 32-months period. Energy Procedia 37, 3267–3274.

Spycher, N., Preuss, K., 2005. CO_2-H_2O mixtures in the geological sequestration of CO_2. II Partitioning in chloride brines at 12-100 C and up to 600 bar. Geochim. Cosmochim. Acta 69 (13), 3309–3320.

Spycher, N., Preuss, K., 2009. A phase-partitioning model for CO_2-brine mixtures at elevated temperature and pressures: application to CO_2-enhanced geothermal systems. Transp. Porous Media 82 (1), 173–196.

Steel, R.J., 1993. Triassic -Jurassic megasequence stratigraphy in the Northern North Sea: rift to post-rift evolution. In: Parker, J.R. (Ed.), Petroleum Geology of Northwest Europe: Proceedings of the 4th Conference. Geological Society, London, pp. 299–315.

Straub, K.M., Paola, C., Mohrig, D., Wolinksy, M.A., Terra, G., 2009. Compensational stacking of channelized sedimentary deposits. J. Sediment. Res. 79, 673–688.

Stride, A. H., Belderson, R. H., Kenyon, N. H., and Johnson, M. A., 1982. Offshore tidal deposits: sand sheet and sand bank facies. In: Stride, A. H. (Ed.) Offshore tidal sands: processes and deposits. New York, Chapman and Hall, 95-125.

Sundal, A., Miri, R., Ravn, T., Aagaard, P., 2015. Modeling CO_2 migration in aquifers; considering 3D seismic property data and the effect of site-typical depositional heterogeneities. Int. J. Greenh. Gas Control 39, 349–365.

Sundal, A., Nystuen, J.P., Rørvik, K.L., Dypvik, H., Aagaard, P., 2016. The Lower Jurassic Johansen Formation, northern North Sea - depositional model and reservoir characterization for CO_2 storage. Mar. Pet. Geol. 7, 1376–1401.

Sundal, A., Hellevang, H., 2019. Using reservoir geology and petrographic observations to improve CO_2 mineralization estimates: examples from the Johansen Formation, North Sea, Norway. Minerals 9 (11), 671.

Sundal, A., Meneguolo, R., Kruber, C., Olsen, E., and Hellevang, H., 2021. Geological storage site assessment: geochemical review of the Aurora Storage Complex, Northern Lights CCS project, North Sea. EAGE CCUS 2021 Putting Carbon Underground. Virtual, 20th April. Extended manuscript in prep.

Swift, D.J.P., 1975. Tidal sand ridges and shoal-retreat massifs. Mar. Geol. 18, 105–134.

Thompson, N.D., Andrews, J.S., Wu, L., Meneguolo, R., 2022. Characterization of the *in-situ* stress on the Horda platform – a study from the Northern Lights Eos well. Int. J. Greenh. Gas Control 114, 103580.

Thompson, N.D., Andrews, J.S., Bjørnarå, T.I., 2021. Assessing potential thermo-mechanical impacts on caprock due to CO_2 injection – a case study from Northern Lights CCS. Energies 14, 5054.

Van den Berg, J.H., Martinius, A.W., Houthuys, R., 2017. Breaching-related turbidites in fluvial and estuarine channels: examples from outcrop and core and implications to reservoir models. Mar. Pet. Geol. 82, 178–205.

Vollset, J., Doré, A.G., 1984. A revised Triassic and Jurassic lithostratigraphic nomenclature for the Norwegian North Sea. Nor. Petrol. Direct. Bull. 3, 2–53.

Walker, R.G., Wiseman, T.R., 1995. Lowstand shorefaces, transgressive incised shorefaces, and forced regressions: examples from the Viking Formation, Joarcam area, Alberta. J. Sediment. Res. B65 (1), 132–141.

Wang, Y., Straub, K.M., Hajek, E.A., 2011. Scale-dependent compensational stacking: an estimate of autogenic time scales in channelized sedimentary deposits. Geology 39 (9), 811–814.

Whipp, P.S., Jackson, C.A.L., Gawthorpe, R.L., Dreyer, T., Quinn, D., 2014. Normal fault array evolution above a reactivated rift fabric; a subsurface example from the northern Horda platform, Norwegian North Sea. Basin Res. 26 (4), 523–549.

Zweigel, P., Arts, R.J., Lothe, A.E., Lindeberg, E., 2004. Reservoir Geology of the Utsira Formation at the First Industrial-scale Underground CO_2 Storage Site (Sleipner area, North Sea), 233. Geological Society, Special Publications, London, pp. 165–180.